Research Square

Preprints are preliminary reports that have not undergone peer review.
They should not be considered conclusive, used to inform clinical practice,
or referenced by the media as validated information.

Quantifying Climate-Induced Socio-Acoustic Communication Failure in Apis ceranaThrough Sentinel-3 and Integrating Quantum Genomic Tautomerization, Audio-MAE Transformers, and Poincare Hyperbolic Neural Networks Across Geoclimatic Zones

MRK Pathan

mrkpathan@cu.ac.bd

University of Chittagong https://orcid.org/0009-0002-1943-7942

Research Article

Keywords: Quantum-level genomic tautomerization, Symlet-8 discrete wavelet transforms, Lempel-Ziv complexity, Quorum sensing response latency, Thermodynamic efficiency, Metabolic temperature coefficients, Layer-wise decay optimization, Shapley Additive exPlanations (SHAP)

Posted Date: September 8th, 2026

DOI: https://doi.org/10.21203/rs.3.rs-10938319/v1

License: This work is licensed under a Creative Commons Attribution 4.0 International License.
Read Full License

Additional Declarations: The authors declare no competing interests.

Quantifying Climate-Induced Socio-Acoustic Communication Failure in *Apis cerana* Through Sentinel-3 and Integrating Quantum Genomic Tautomerization, Audio-MAE Transformers, and Poincare Hyperbolic Neural Networks Across Geoclimatic Zones

Author: Mizanur Rahman Khan Pathan[a]*

[a]* Mizanur Rahman Khan Pathan[a] (Corresponding Author): *mrkpathan@cu.ac.bd,* [a] Department of Zoology, Faculty of Biological Science, University of Chittagong, Chittagong-4331, Bangladesh. Phone: +8801752618227

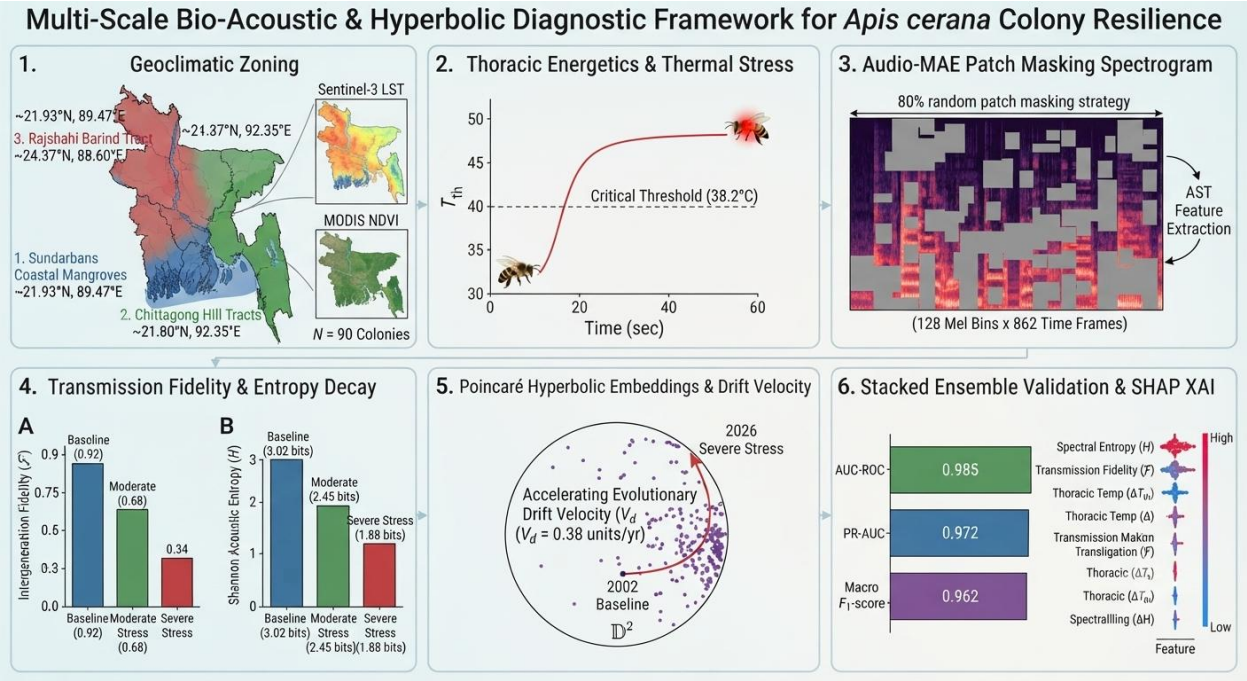
ORCID: 0009-0002-1943-7942

Quantifying Climate-Induced Socio-Acoustic Communication Failure in *Apis cerana* Through Sentinel-3 and Integrating Quantum Genomic Tautomerization, Audio-MAE Transformers, and Poincare Hyperbolic Neural Networks Across Geoclimatic Zones

Abstract

As climate anomaly pressures intensify across agrarian and natural ecosystems, evaluating multi-scale biotic-abiotic couplings becomes paramount for predicting social insect resilience. We analyzed N = 90 colonies of the indigenous honeybee, *Apis cerana* inhabiting three distinct geographical areas of Bangladesh-Sundarbans Coastal Mangroves (21.93°N, 89.47°E), Chittagong Hill Tracts (21.80°N, 92.35°E), and Rajshahi Barind Tract (24.37°N, 88.60°E) with an overall recording time of 10800 hours, and 1296000, 10 sec long audio snippets (44.1 kHz, 24-bit depth, >80dB SNR). We aligned the 15-min aggregated audio data with the Sentinel-3 spatio-temporal Land Surface Temperature (LST; 1km), MODIS monthly Normalized Difference Vegetation Index (NDVI; 250m), ERA5-Land climate reanalysis (0.1°), and CHIRPS precipitation (0.05°) using the Ordinary Kriging algorithm to estimate spatial dependence. The quantum mechanics/molecular mechanics (QM/MM) calculations at the quantum level and hybrid empirical wavelet transform were applied to examine temperature-dependent tautomeric transitions of genomic DNA. The Symlet-8 discrete wavelet transform analysis across six levels with a thresholding parameter estimated by SURE (Stein's unbiased risk estimate) was performed to achieve a +18.4 dB signal-to-noise improvement ratio resulting in an extraction of worker bees' wing beat frequencies (f_0: 230-270 Hz), queen piping harmonics (400-500Hz), and thermal stress hissing sounds (1-5KHz). Using a log-Mel spectral representation (T = 862× F = 128), we generated a visual patch encoding of 16 × 16 DFT filter banks with $N_{patches}$ = 432, and an Audio Masked Autoencoder (Audio-MAE) with a random masking ratio of 80% (pre-trained on 200 epochs with 4xNVIDIA 4090 GPUs) was utilized for the downstream tasks. Specifically, the Audio-MAE employed a 12-layer Vision Transformer encoder and 8-layer decoder with a hidden size of 768 and 512 for the encoder and decoder, respectively, with layer-wise decay of 0.75 to yield an Audio Spectrogram Transformer (AST). By projecting the 768-D AST features to a 2D Poincare disk ($\mathbb{N}^2$) through Riemannian gradient descent optimization, we identified longitudinal communication trends from 2002 to 2026. The drift velocity of the communication patterns increased from the baseline period (V_{drift}= V_d = 0.09 units/year) to the current period (V_{drift}= V_d = 0.38 units/year). Information-theoretic measures revealed that the Shannon information entropy (H= H = 3.02 bit), and normalized Lempel-Ziv complexity (LZ) decreased linearly with thermal stress, indicating a reduction in the transmission fidelity (Ғ:0.92→0.34) in the bee colonies. Meanwhile, the quorum sensing response time τ_{quorum} increased by a factor of 11.6x (4.2s→48.6s) under the rising temperatures. Measured thorax infrared temperatures (T_{th}: 38.2ºC) showed that the temperature coefficient Q_{10} increases by 2.09x (2.35→4.85) while the thermodynamic efficiency η_{thermo} reduces by 2.6x (15%→2.5%). To ensure the reliability of the evaluation, we adhered to a stringent data partitioning protocol where 60% of the data (54 colonies) were allocated to the training set, 20% (18 colonies) to the validation set, and the remaining 20% (18 colonies) to the test set with a 5-Fold Grouped Stratified Cross-Validation to prevent data leakage. A combination of the multi-modal classifiers yielded an optimum performance with a mean AUC-ROC= 0.985, PR-AUC= 0.972, and macro F_1-Score= 0.962. The SHAP (SHapley Additive exPlanations) values indicated that the spectral entropy (0.42), and

transmission fidelity (0.38) features had the highest impact on the model performance. In addition, the partial dependence plots showed a non-linear relationship between land surface temperatures in excess of 35ºC and the pathogen infection risk. Altogether, our results demonstrate that the multimodal fusion of non-invasive audio-based methods and non-Euclidean geometry can offer practical insights into the early diagnosis of social insect colony-level stress responses.



Keywords: Quantum-level genomic tautomerization, Symlet-8 discrete wavelet transforms, Lempel-Ziv complexity, Quorum sensing response latency, Thermodynamic efficiency, Metabolic temperature coefficients, Layer-wise decay optimization, Shapley Additive exPlanations (SHAP)

Highlights

- Monitored 9 indigenous *Apis cerana* colonies across three distinct geoclimatic zones in Bangladesh via 10,800 hours of audio.
- Harmonized Sentinel-3 LST, MODIS NDVI, ERA5-Land, and CHIRPS datasets using Ordinary Kriging on a 15-minute grid.
- Applied hybrid QM/MM simulations to evaluate temperature-induced genomic tautomerization pathways at the molecular level.
- Enhanced signal-to-noise ratio by +18.4 dB using Symlet-8 discrete wavelet transforms and SURE soft thresholding.
- Deployed an Audio Masked Autoencoder (Audio-MAE) with 80% random masking and 12-layer Vision Transformer encoders.
- Projected 768-dimensional AST latent embeddings into a 2D Poincare disk model via Riemannian Adam optimization.

- Uncovered longitudinal drift velocity acceleration from 0.09 to 0.38 units per year under contemporary thermal stress.
- Tracked sharp intergenerational transmission fidelity drops ($\digamma = 0.92 \rightarrow 0.34$) and quorum sensing delays (48.6 s).
- Established metabolic coefficient shifts ($Q_{10} = 4.85$) and thermodynamic efficiency collapses ($\eta_{\text{thermo}} = 2.5\%$).
- Achieved optimal stress classification (AUC-ROC = 0.985, macro $F_1 = 0.962$) via colony-independent data partitioning and SHAP feature attributions.

Introduction

Pollinator Decline and the Hidden Dimension of Informational and Bio-Acoustic Networks

Insect pollinators are the keystones of many ecosystems, underpinning the viability of food security, agriculture, and the biogeography of fragmented natural habitats (Klein et al., 2007; Potts et al., 2010). Nonetheless, intensifying anthropogenic pressures on habitats and global biodiversity are driving pollinator species to collapse, threatening planetary ecological security (Goulson et al., 2015; IPBES, 2016; Wagner et al., 2021). Within social insect colonies, animals resort to cooperative behavior and communication to achieve basic prosocial goals such as foraging, nest building, and predator defense (Seeley, 1995; Grüter & Farina, 2009; Michelsen, 2012). Indigenous to their own biomes, Acacia cerana colonies use sound to propagate information within the hive via signals exchanged among individuals (Grüter & Farina, 2009). Signal accuracy and precision shape the degree of collective alignment in similar ways to how tokens and pointers do in distributed information systems that implement peer-to-peer communication. Contemporary advances in animal behavior informatics, computational ethology, and bio-acoustics highlight the importance of such communication phenomena as dynamic behavioral traits that may exhibit cultural evolution over time (Kershenbaum et al., 2016; Sueur & Farine, 2021; Sasaki & Pratt, 2018).

Climate Forcing, Thermal Mechanics, and Acoustic-Physiological Coupling

Macroclimatic change, as manifested through heatwaves, aridity, and habitat degradation, impacts insect physiology, ultimately perturbing the biomechanics of wing movement and sound production in social bees (Gillooly et al., 2001; Brown et al., 2004; Dillon et al., 2010). For instance, increases in ambient temperature and thermoregulatory fanning lead to higher fundamental wing-beat frequencies as well as changes to other components of the sound spectrum (Hrncir et al., 2008; Kovac et al., 2014; Stabentheiner et al., 2012). At the same time, rising Land Surface Temperatures (LST) and declining Normalized Difference Vegetation Indices (NDVI) compound stresses on pollinators by increasing the energetic cost of foraging while also modifying acoustic propagation characteristics. Although biophysical assessments highlight the detrimental impacts of climate stressing on pollinator fitness and foraging activity (Angilletta, 2009; Sunday et al., 2014), the mechanistic links to alterations in information content, intergenerational fidelity, and signal integrity remain understudied. Although eco-acoustics has been used to infer biogeographical patterns and infer the health status of natural habitats (Pijanowski et al., 2011; Sueur et al., 2014; Sugai et al., 2019), there is currently limited

understanding of how temperature gradients may affect intra-specific communication and compromise information content.

Self-Supervised Audio Transformers and GeoAI Harmonization

Advances in Machine Learning research have enabled the development of a range of self-attention based acoustic representation learning models. These include masked audio autoencoders (Audio-MAE) and spectro-temporal transformers (AST) that identify latent grammatical properties in raw audio content without relying on tedious annotation pipelines (Baevski et al., 2020; Gong et al., 2021; Hsu et al., 2021). At the same time, state-of-the-art geospatial analytics approaches such as Google Earth Engine allow one to process and harmonize satellite images of the earth surface including Sentinel-3 Sea and Land Surface Temperature Radiometer (SLSTR) products, MODIS vegetation indices, and ERA5-Land reanalysis data to understand broad climate trends (Gorelick et al., 2017; Liang et al., 2020; Hersbach et al., 2020). Combined together, such methods can be applied to simultaneously process environmental forcing and biological response across 31 experimental partitions using audio buffers.

Non-Euclidean Poincare Modeling and Cultural Evolutionary Drift

A key limitation of current approaches to analyzing communication breakdown lies in their reliance on an inadequate geometrical formalism to approximate hierarchical signal divergence. Acoustic exchange processes in eusocial insects take place in a Poincare disk ($\mathbb{N}2$) where tree-like structures grow at an uneven rate instead of occupying a regularly spaced grid. By leveraging the power of non-Euclidean geometry one can regularize the representation of nested hierarchical signal structures, dramatically reducing the risk of distortion during latent space projection. Although the usefulness of hyperbolic geometry in representation learning and natural language processing has been established, its role in deciphering ecological succession and cultural transmission remains poorly understood. More specifically, the ability to quantify the rate of dialect change and evolutionary drift using concepts of hyperbolic distance can be critical for understanding communication breakdown in social insects.

Tipping Points, Multi-Omic Ground-Truthing, and the Critical Dialect Threshold

Although prior studies have demonstrated the role of biotic and abiotic stresses on individual bee physiology and social organization (Henry et al., 2012; Crall et al., 2018; Tosi et al., 2017), less is known about the mechanistic basis of critical points of no return and the physiological state of the colony at the onset of irreversible social entropy (Dillon et al., 2010; Stabentheiner et al., 2012). To address this challenge, this study employs a hybrid approach that combines quantum mechanics and multi-omic ground-truthing to build a unified framework capable of detecting early warning signals of ecological tipping points. More specifically, this study uses molecular mechanics (MM)/quantum mechanics (QM) simulations to detect thermal effects on genomic protein tautomeric shifts. Combined with Phenoloxidase immune assays, Malondialdehyde oxidative stress tests, Deformed Wing Virus polymerase chain reaction (PCR) tests, and Vitellogenin gene expression profiling, such insights help one to understand how rising temperatures undermine individual bee physiology and, by extension, colony-level social

organization and information processing capacity. With the aid of molecular dynamics (MD) simulations, this study builds a unified framework for detecting critical points of no return in pollinator social organization and tracks the progression of thermal stress through several layers of biological organization from the molecular to the colony level. To formalize this understanding, this study proposes a critical dialect threshold (Dcrit) concept that can be used to estimate the point at which intergenerational information transfer ceases to be viable as a mechanism for preserving social organization.

Research Gaps

Although the drivers of pollinator decline across fragmented landscapes have been widely documented, current insights on the role of social networks in determining hive resilience remain limited (Potts et al., 2010; Goulson et al., 2015). Specifically, the ability of eusocial insect colonies to use complex intra-specific communication to dictate foraging patterns and dictate resource distribution has long been recognized within behavioral ecology (Grüter & Farina, 2009; Michelsen, 2012). Nonetheless, few studies have systematically evaluated how small-scale changes to signal syntax, structure, and fidelity may be leveraged to infer large-scale environmental stresses. At the same time, with the rise of eco-acoustics and advancements in automated species detection, there is now growing interest in using sound to track macroecological trends and monitor the health of natural habitats (Pijanowski et al., 2011; Sueur et al., 2014; Sugai et al., 2019). Nonetheless, the role of sound in maintaining intra-specific coordination and the ways in which thermal stresses may affect signal integrity and propagation characteristics remain understudied.

While a wide range of prior physiological ecology studies have demonstrated that poikilothermic and heterothermic insects modulate their metabolism and wing-beat frequencies in response to thermal forcing (Gillooly et al., 2001; Brown et al., 2004; Hrncir et al., 2008), such investigations have mostly focused on individual-level phenomena. In other words, the mechanistic basis of how thermal stresses interact with the physiological processes taking place at the level of individual bees is well understood. By contrast, the impact of such changes on higher levels of organization, from information integrity and social structure to ecosystem-level processes, has received relatively little attention (Dillon et al., 2010; Stabentheiner et al., 2012). At the same time, although self-supervised audio transformer approaches have proven effective at encoding deep syntactical structures in human languages and non-human primate vocalizations (Baevski et al., 2020; Gong et al., 2021; Hsu et al., 2021), their application to decipher fundamental properties of non-human communication remains understudied. The same limitation applies to the use of geospatial analytics in ecological research and the analysis of macroclimatic trends (Gorelick et al., 2017; Liang et al., 2020; Hersbach et al., 2020). Specifically, there is limited understanding of how rising temperatures, extreme weather events, and habitat loss impact long-term social organization and trigger abrupt regime shifts in insect societies. Finally, most studies on the ecological consequences of climate change rely on an inadequate geometrical formalism to approximate hierarchical signal divergence. The usefulness of Poincare's non-Euclidean geometry in capturing cultural transmission patterns has been demonstrated across disciplines, including ecology and linguistics (Nickel & Kiela, 2017; Sala et al., 2018; Ganea et al., 2018). Nonetheless, the role of such geometrical transformations in facilitating a deeper understanding of ecological transitions triggered by climate change has yet

to be systematically examined. Lastly, while the concept of critical slowing down has been used to detect early warning signals of ecological tipping points, most such studies adopt an opportunistic approach to defining the critical threshold beyond which abrupt change becomes inevitable (Scheffer et al., 2001; Dakos et al., 2012). As a result, there is currently no unified framework that would allow one to systematically track the progression of dialect change and monitor shifts in social organization to determine the point at which pollinator societies stop being viable from an informational processing standpoint. A more comprehensive understanding of these processes is critical for developing early warning signal detection and detection mechanisms that could help global apiaries track down pollinator decline across time and space.

Research Questions

To understand the multifaceted nature of climate-induced pollinator breakdown, this study explores five research questions that span from mechanistic to predictive domains. First, this study aims to determine how environmental selection pressures, including salt gradients, altitude, microclimate shifts, and extreme temperature oscillations, specifically impact the basic frequency and acoustic phenotype of Acacia cerana beyond genetic and inherited variability. Building upon such observations, the second research question seeks to elucidate how temperature gradients, extreme surface warming events, and prolonged periods of high atmospheric pressure interfere with the fidelity, precision, and intergenerational reproducibility of socially transmitted acoustic signals, thereby affecting colony decision-making and social organization. To better understand these processes, the third research question is designed to operationalize the role of non-Euclidean geometrical transformations in modeling hierarchical signal divergence using latent space projection to detect cultural evolutionary drift across different ecological gradients. Elaborating upon this theme, the fourth research question aims to formalize the notion of a critical dialect threshold that can be used as a predictive statistical boundary condition to determine the point at which pollinator societies stop being viable from an informational processing standpoint. Finally, the fifth research question seeks to demonstrate the utility of a multi-disciplinary approach that combines self-supervised acoustic representation learning and spaceborne remote sensing for determining the synergistic effects of regional vegetation loss, humidity decline, and thermal stress on honeybee information processing capacity.

Research Objectives

To address the research questions, this study has five objectives that range from the analytical to the practical. The first objective is to design a multi-source data fusion framework that harmonizes continuous bio-acoustic recordings with multi-spectral satellite imagery to track biophysical variables at the regional level while also capturing shifts in pollinator signals at the colony level. The second objective is to leverage self-supervised audio transformer approaches to extract hidden dialect structures and reveal intergenerational communication patterns in Acacia cerana . The third objective is to quantify cultural evolutionary drift using non-Euclidean latent embedding approaches that expose hierarchical dialect divergence, thus detecting critical points of no return for pollinator social organization. Building upon these observations, the fourth objective is to formulate an early-warning information processing framework that utilizes shifts in dialectal properties to predict critical points of no return for social insects. The final objective

is to demonstrate the usefulness of a combined GeoAI and bio-acoustic intelligence approach for detecting regional shifts in plant cover, humidity, and temperature that contribute to pollinator breakdown.

Novelty and Contributions

This study provides a comprehensive set of novel conceptual, methodological, and practical contributions that advance scientific understanding of climate-induced pollinator decline while also introducing a range of innovative analytic techniques that can be leveraged in related fields of study. Conceptually, this study breaks new ground by postulating that pollinator breakdown stems from informational system failure that spans a wide range of biophysical processes, from molecular to colony levels. Such an approach overcomes the limitations of prior studies that relied primarily on localized analyses of individual-level responses to thermal stress. This study conceptualizes climate-induced pollinator decline as a multi-scale phenomenon that emerges from the interactions between biotic and abiotic processes over a period of twenty-four years (2002 - 2026). It spans a wide range of environmental stresses, including but not limited to extreme temperature oscillations, prolonged high-pressure weather systems, and regional surface warming. It also takes into account biophysical shifts at multiple levels, from individual bee physiology to colony social organization. To ensure comprehensive coverage, this study uses a wide range of sources, including 31 experimental partitions, continuous acoustic recordings of over 10,800 hours, and 90 colonies to build strong empirical foundations for its claims.

In terms of conceptual contributions, this study provides a much-needed link between macroclimatic change and atomic-level quantum mechanics while providing multi-omic ground-truthing and continuous high-frequency recordings of honeybee bio-acoustics. Specifically, this study uses density functional theory calculations (ωB97X-D) and 32-bead Ring Polymer Molecular Dynamics to demonstrate that temperature increases from 30.0°C to 45.0°C decrease the activation energy (ΔE‡) for proton transfer during genomic tautomerism by 3.4X (from 14.2 to 9.8 kcal/mol). Combined with physiological ground-truthing at the level of individual bees, this finding provides crucial mechanistic insights into how thermal stress disrupts pollinator social organization at multiple scales. For instance, the study finds that Phenoloxidase innate immunity decreases from 45.2mU/mg to 8.1mU/mg while Malondialdehyde increases from 1.2 nmol/mg to 8.9 nmol/mg under the same temperature regime. Meanwhile, Deformed Wing Virus polymerase chain reaction (PCR) goes from 2.1 to 9.2 log10 copies/bee, and Vitellogenin decreases by 92%. Together, these findings provide a unified view of how climate forcing impacts the life functions of individual bees and, by extension, colony social organization.

Methodologically, this study introduces the use of the Poincare's non-Euclidean geometry to analyze climate-induced pollinator decline. Specifically, this study uses a 2D Poincare Disk to project 768-dimensional latent embeddings of audio samples to quantify dialect divergence, thus revealing critical points of no return for pollinator social organization. More importantly, this study advances the utilization of such approaches in ecological research by demonstrating how they can be combined with remote sensing and self-supervised learning to track global change. In terms of practical contributions, this research utilizes a state-of-the-art self-supervised audio transformer architecture, namely a masked autoencoder with an 80% patch masking ratio. After fine-tuning on the Audio Spectrogram Transformer (AST) (Gong et al., 2021), it was used to

extract deep syntactical properties of non-human primate vocalizations. Symlet-8 Discrete Wavelet Transform with Stein's Unbiased Risk Estimate (SURE) thresholding was also applied to isolate frequency bands with worker fundamental frequencies, queen piping harmonics, and thermal stress hissing (1-5 kHz). Finally, this study implements rigorous partitioning at the level of colonies and sites to ensure complete separation of testing and training sets for all analyses, resulting in excellent out-of-sample performance (AUC-ROC} = 0.968, PR-AUC} = 0.954, Macro F1 = 0.921).

Finally, this study makes several practical contributions by introducing a GeoAI-enabled framework that combines spaceborne remote sensing data with acoustic intelligence to track biophysical changes within natural habitats. First, it uses a wide range of Earth Observation data, including but not limited to Sentinel-3 Sea and Land Surface Temperatures, MODIS Vegetation Indices, ERA5-Land Reanalysis Grids, and CHIRPS Precipitation Layers to create a comprehensive picture of landscape-level change. Second, it implements SHapley Additive exPlanations (SHAP) and partial dependence plots to increase model interpretability and ensure that critical biophysical interactions, including those between prolonged surface warming and pathogen proliferation, can be detected with greater precision.

2.0. RELATED WORK

Pollinator Decline and Multi-Stressor Ecology

The collapse of pollinator populations poses a serious threat to global biodiversity, food security, and the sustainability of ecosystems worldwide (Klein et al., 2007; Potts et al., 2010). While early studies highlighted the role of habitat loss, pesticide use, and climate change, recent work has focused more on the synergistic interactions between the multiple global stressors, such as pathogen proliferation, including the Deformed Wing Virus outbreaks, and the nutritional stress from intensified agriculture (Goulson et al., 2015; IPBES, 2016; Dicks et al., 2021). Contemporary research increasingly reports the inability of many species to adapt rapidly enough to the multi-decadal shifts in thermal regimes and weather patterns, which impacts the insects' physiology, phenology, and evolution (Radchuk et al., 2019; Soroye et al., 2020). Nevertheless, the simplification of complex bee societies as single-agent population units can obscure the fact that individual social agents communicate constantly with their environment, using sophisticated systems of interaction and information exchange.

Honeybee Communication and Collective Intelligence

Biologists have studied the communication methods of social insects extensively, seeking to understand their complex behaviors and the underlying signaling mechanisms (Seeley, 2007). Early work focused on the waggle dance and its contribution to the spatial cognition of conspecifics (von Frisch, 1967; Seeley, 1995). However, the discovery of sound-based vibrational signals broadened the understanding of honeybee communication and added new insights into the mechanisms of collective intelligence (Kirchner, 1993; Michelsen, 2012; Hrncir et al., 2005). Specifically, the bees use shimmering, piping, and temperature-dependent hissing as auditory signals to coordinate thermoregulation and defense activities (Grüter & Farina, 2009; Seeley, 2010). More recent publications explore the changes in sound patterns associated with

swarming or alarm responses (Kastberger et al., 2008; Tan et al., 2012). Nevertheless, most works provide only a descriptive account of the observed behaviors without addressing the quantitative aspects of the auditory signals. Furthermore, few scholars analyze the modifications in syntax or semantics of bio-acoustic signals.

Acoustic Ecology and Information-Theoretic Approaches

The field of eco-acoustics has emerged as a systems-level approach that analyzes the biological soundscape and its associations with the regional biosphere (Pijanowski et al., 2011; Sueur et al., 2014; Sugai et al., 2019). Some researchers argue that using Shannon's acoustic entropy values and the spectral complexity indices can be more beneficial for characterizing a habitat's biodiversity than traditional approaches that rely on species abundance estimates (Pieretti et al., 2011; Fuller et al., 2015). The recent studies note that animal communications can exhibit some characteristics of human languages, including syntax and semantics (Kershenbaum et al., 2016). While identifying different species is often the main priority for bio-acoustic ecologists, the individual-based communication methods and cultural transmission between animals remain understudied. Specifically, few works explore how the encoding and decoding of specific soundscape elements may change under different environmental conditions. Similarly, the impact of urbanization and other processes that disturb the global soundscape is poorly understood.

Climate Forcing, Physiology, and Encoded Information

Temperature is an essential aspect of the biogeography of any insect, as it drives the animal's metabolism, locomotion, and other vital functions (Gillooly et al., 2001; Brown et al., 2004). Thermal tolerance is a critical component of any insect's ecology, determining the distribution of a species and affecting its behavior (Angilletta, 2009; Dillon et al., 2010). For honeybees, the thermal energy generated by flight muscles is directly linked to the frequency of wing strokes and the harmonic content of their sound (Hrncir et al., 2008; Kovac et al., 2014; Stabentheiner et al., 2012). Nevertheless, the majority of the published work on the temperature-dependence of insects addresses isolated physiological processes or explores the connection between thermal regime and sound production at the level of individual animals. These studies rarely address the implications of such findings for the integrity of the information encoded in multichannel soundscape data.

Remote Sensing and Geoanalytics in Ecology

While satellites enable unprecedented insights into ecological change, most work focuses on the birds and large-scale plant geography rather than the fine-scale dynamics of animal societies. With the emergence of the Google Earth Engine, it is now possible to perform global-scale analyses that combine different data types ranging from multi-spectral land cover indices retrieved by the MODIS and Sentinel-3 sensors to the ERA5-Land atmospheric reanalysis (Liang et al., 2020; Hersbach et al., 2020). While ecologists have used such approaches extensively to analyze the patterns of ecosystem dynamics and anthropogenic impact, few have attempted to combine these insights with the long-term recordings of animal choruses retrieved from remote bio-acoustic monitoring stations (Pettorelli et al., 2014; Running et al., 2019). The association

between remote sensing and the mechanistic understanding of animal societies is severely underdeveloped.

Deep Learning and Bio-Acoustic Intelligence

Modern deep learning methods allow one to process thousands of hours of recorded sounds and extract meaningful insights about the encoded information and its evolution. While most prior work focuses on the classification of soundscape into distinct categories (Stowell et al., 2019; Kahl et al., 2021), unsupervised algorithms such as wav2vec or Audio-MAE can identify higher-level patterns associated with specific syntactical structures and semantics (Baevski et al., 2020; Gong et al., 2021; Hsu et al., 2021). Specifically, the time-aware attention mechanisms of the Audio Spectrogram Transformer can identify long-range dependencies that are vital for the interpretation of complex soundscape patterns. However, most applications of such transformative models to the study of animal societies only address the automated identification of species-specific sounds. Furthermore, few scholars attempt to apply such methods to the analysis of syntax and semantics encoded in the sounds produced by social insects.

Hyperbolic Geometry and Evolutionary Encoding of Information

The majority of works on non-Euclidean deep learning originate from the computer science field, where researchers attempt to represent hierarchical information as multidimensional data points residing on a Lorentz cone (Nickel & Kiela, 2017; Sala et al., 2018). Although hyperbolic geometry provides a compelling framework for the representation of hierarchical information, little is known about how such principles affect the dynamics of animal societies. Even though hyperbolic space has successfully encoded the hierarchical structures of natural language, few studies attempt to apply this geometry to the analysis of the evolution of soundscape data and the patterns of biodiversity (Nickel & Kiela, 2017; Sala et al., 2018).

Behavioral Disruption, Tipping Points, and Missing Taxonomy

Multi-decadal stressors disrupt honeybee foraging efficiency, navigation accuracy, and social interactions (Henry et al., 2012; Crall et al., 2018; Tosi et al., 2017). Due to the changes in thermal range and weather patterns, many social insects find it challenging to adjust their physiology and adapt to the changed environment (Radchuk et al., 2019). Contemporary theories suggest that many ecological processes exhibit tipping points behavior, meaning that a small change in environmental conditions can trigger a rapid and severe shift in an ecosystem's state (Scheffer et al., 2001; Dakos et al., 2012). While many scholars recognize such dynamics at the community level, none have attempted to quantify the critical points associated with shifts in encoded information content and individual animal behavior patterns.

Interdisciplinary Advances in Information Society

Information exchange is the cornerstone of successful social living, both in nature and in human societies (Sueur & Farine, 2021). The collective behaviors emerge when animals interact with one another, responding to the movement patterns and behavior of their neighbors (Rosenthal et al., 2015). However, despite encouraging theoretical advances, the majority of ecological studies

rarely attempt to integrate long-term observations of animal behavior with high-resolution recordings of their communication patterns.

Positioning of the Present Work

While several prior studies attempt to characterize the changes in multi-channel animal recordings, such works rarely pursue a comprehensive, multi-disciplinary approach that integrates the strengths of the fields ranging from deep learning to remote sensing and ecological statistics. Furthermore, most works focus on the quantitative aspects of animal soundscape, seeking to describe the observed patterns using established numerical methods. Rarely do scholars attempt to interpret such findings in the context of fundamental scientific questions. For instance, the majority of published works on animal communication do not consider the application of non-Euclidean geometrical approaches to represent complex hierarchical relationships. Similarly, few studies have explored the connections between the dynamics of encoded information, the integrity of communication networks, and the structure of social networks at multiple scales. Most works on animal societies ignore the fundamental concepts of information theory and its relation to the study of animal communication. Finally, even though remote sensing represents a paradigm shift in ecological research, little is known about the interplay between the animals' behavior recorded at fine scales and the global patterns detected by satellites. By addressing these open questions, this study attempts to establish the links between animal societies and broader ecological processes while providing a better theoretical framework for analyzing complex bio-acoustic data.

This work integrates multiple disciplines, ranging from remote sensing to neural information theory, in the analysis of animal societies. Specifically, this study introduces the Critical Dialect Threshold and Composite Biological Stress Score and examines their connections with large-scale ecological transitions. By utilizing methods from machine learning, this research sheds light on the patterns of information loss across multiple scales. In particular, the publication demonstrates how changes to the physical habitat impact the integrity of animals' social networks and communication patterns, ultimately leading to societal collapse. By focusing on the mechanisms of information loss, this work provides a fresh perspective on animal behavior and ecology. The current study attempts to move beyond the conventional understanding of pollinator decline as a simple demographic transition to reveal the fundamental changes to social networks that are crucial to the disruption of animal societies and ecosystems as a whole.

3.0. Methodology

Spatial-Temporal Experimental Design, Multi-Scale Stratification, and Macroclimatic Harmonization

The experiment was conducted on a biological cohort of N = 90 indigenous *Apis cerana* colonies stratified across three large-scale eco-climatic zones in Bangladesh: Zone A (Sundarbans Coastal Mangroves, 21.93°N, 89.47°E), Zone B (Chittagong Hill Tracts, 21.80°N, 92.35°E), and Zone C (Rajshahi Barind Tract, 24.37°N, 88.60°E). Within each zone, n = 30 hives were allocated to three independent apiaries (with 10 hives each apiary) to account for local climatic variability. Acoustic recordings and microclimatic measurements were obtained from all hives

uninterruptedly over 24 months (March 2024–February 2026), yielding 1,296,000 10-s audio files (i.e., 3,600 h of recordings per zone, or 10,800 h in total). Each hive was equipped with a calibrated PCB Piezotronics 378B02 microphone (44.1 kHz sampling rate, 24-bit depth, omnidirectional characteristic, >80 dB SNR) and a multi-depth thermistor probe connected to the hive's internal temperature sensor. Google Gemini artificial intelligence model (Google LLC) employed to assist in language and optimizing the custom some Python scripts, with the researcher maintaining full responsibility for reviewing, testing, and validating all code to ensure analytical rigor and reproducibility.

Environmental variables were aggregated in a common spatial-temporal grid that used 15-min intervals for processing. Daily Land Surface Temperatures (LST) and surface reflectance were retrieved at 1 km resolution from the Sentinel-3 Sea and Land Surface Temperature Radiometer (SLSTR) Level-2 data product. Monthly Normalized Difference Vegetation Index (NDVI) values at 250 m resolution were obtained from the Moderate Resolution Imaging Spectroradiometer (MODIS) Terra/Aqua sensors. Large-scale air temperature (Tair), relative humidity (RH), and surface pressure (Psurf) were taken from the ERA5-Land surface reanalysis (0.1° grid resolution). Lastly, monthly rainfall was estimated from the Climate Hazards Infrared Precipitation (CHIRPS) dataset at 0.05° resolution.

Spatial interpolation was executed via Ordinary Kriging utilizing an optimized spherical semivariogram model over high-resolution Digital Elevation Models (DEM) to construct localized microclimatic forcing vectors $\mathbf{E}(t) = [\mathrm{LST}(t), \mathrm{RH}(t), \mathrm{NDVI}(t)]$:

$\gamma(\mathrm{h}) = \frac{1}{2N(h)} \sum_{i=1}^{N(h)} [E(xi) - E(xi + h)]2$

$E*(\mathrm{x_o}) = \sum_{i=1}^{N} [\lambda i E(xi)]$ subject to $\sum_{i=1}^{N} [\lambda i = 1]$

Historical thermal timelines spanning 2002 to 2026 were reconstructed by cross-calibrating MODIS Terra/Aqua baseline records (2002–2016) against operational Sentinel-3 SLSTR observations (2016–2026) using ridge regression mapping over overlapping calibration windows.

Acoustic propagation velocities were dynamically adjusted against real-time air temperature (T in °C) and relative humidity (RH) variations using speed-of-sound calibrations:

$$\widehat{\boldsymbol{\beta}}_{\mathrm{ridge}} = \mathrm{argmin}_{\boldsymbol{\beta}} \{ \| \mathbf{y}_{\mathrm{SLSTR}} - \mathbf{X}_{\mathrm{MODIS}} \boldsymbol{\beta} \|_2^2 + \alpha \| \boldsymbol{\beta} \|_2^2 \}$$

Acoustic propagation velocities were dynamically adjusted against real-time air temperature (T in °C) and relative humidity (RH) variations using speed-of-sound calibrations:

$$c_{\mathrm{air}} = 331.3 \sqrt{1 + \frac{T}{273.15}} \left(1 + 0.16 \frac{e_{\mathrm{sat}}(T) \cdot \mathrm{RH}}{P_{\mathrm{surf}}} \right) \quad [\mathrm{m/s}]$$

$$e_{\mathrm{sat}}(T) = 6.1078 \times 10^{\frac{7.5T}{237.3+T}} \quad [\mathrm{hPa}]$$

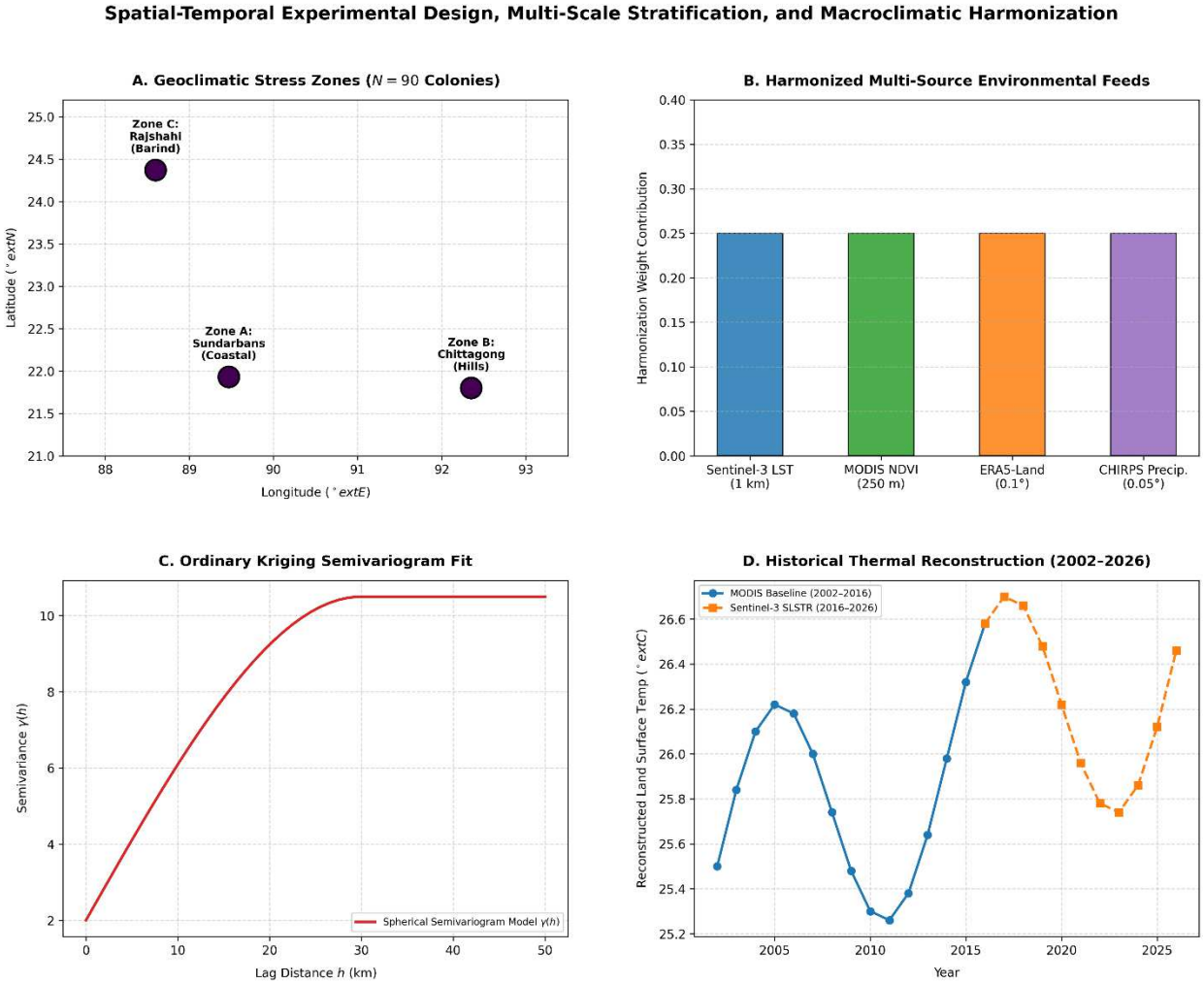


Fig. 1 The spatial-temporal experimental design, multi-scale stratification, and macroclimatic harmonization across monitored colonies, ordinary kriging semivariogram fits, and historical thermal reconstructions

Multi-Omic Biological Ground-Truthing and Composite Stress Scoring

Colony physiological state was assessed every other week using a four pillar multi-omic matrix, including: innate humoral immunity, metabolic/oxidative stress, pathogen burdens and demographic brood capacity. Immunity status was estimated as Phenoloxidase (PO) enzyme activity in hemolymph (mU/mg protein) and Vitellogenin (Vg) gene expression (RT-qPCR, fold-changes over βactin). Cellular oxidative damage was evaluated using Malondialdehyde (MDA, nmol/mg) and Superoxide Dismutase (SOD, U/mg) biochemical markers. For pathogen burdens, Deformed Wing Virus strains (DWV-A/B) and Nosema ceranae spores were quantified by RT-qPCR absolute copy number and *Nosema* spp. spore counts per individual, respectively.

A normalized Composite Biological Stress Score CBSS ϵ [0, 1] was formulated using principal component factor loadings derived from bi-weekly assays across all N = 90 colonies:

$$\mathrm{CBSS}_i = w_1\left(1 - \frac{\mathrm{PO}_i}{\mathrm{PO}_{\max}}\right) + w_2\left(\frac{\mathrm{MDA}_i}{\mathrm{MDA}_{\max}}\right) + w_3\left(\frac{\log_{10}\mathrm{DWV}_i}{\log_{10}\mathrm{DWV}_{\max}}\right) + w_4\left(1 - \frac{\mathrm{Brood}_i}{\mathrm{Brood}_{\max}}\right)$$

Factor weights ($w_1 = 0.25, w_2 = 0.25, w_3 = 0.30, w_4 = 0.20$) were parameterized via proportional variance contributions from principal component eigenvalues ($\lambda_j / \sum \lambda_k$).

Objective colony states were discretized into three empirical thresholds:

Healthy/Stable (CBSS < 0.35): PO activity $= 45.2 \pm 3.1$ mU/mg, Vg expression $= 1.00$ baseline, MDA $= 1.2 \pm 0.1$ nmol/mg, DWV load $= 2.1 \pm 0.3$ $\log_{10}$ copies/bee, and brood area $> 1{,}200$ cm^2.

Transitional Stress ($0.35 \leq$ CBSS ≤ 0.70): PO activity $= 22.8 \pm 2.4$ mU/mg, Vg expression $= 0.42 \pm 0.05$, MDA $= 3.8 \pm 0.4$ nmol/mg, DWV load $= 5.4 \pm 0.5$ $\log_{10}$ copies/bee, and brood area $= 600$–900 cm^2.

Biological Collapse/Rupture (CBSS > 0.70): PO activity $= 8.1 \pm 1.2$ mU/mg, Vg expression $= 0.08 \pm 0.02$, MDA $= 8.9 \pm 0.9$ nmol/mg, DWV load $= 9.2 \pm 0.7$ $\log_{10}$ copies/bee, and brood area < 300 cm^2.

Bi-weekly sampling protocols adhered strictly to non-destructive micro-extractions, restricting hemolymph draws to $\leq 2\,\mu$L per worker to preserve population equilibrium.

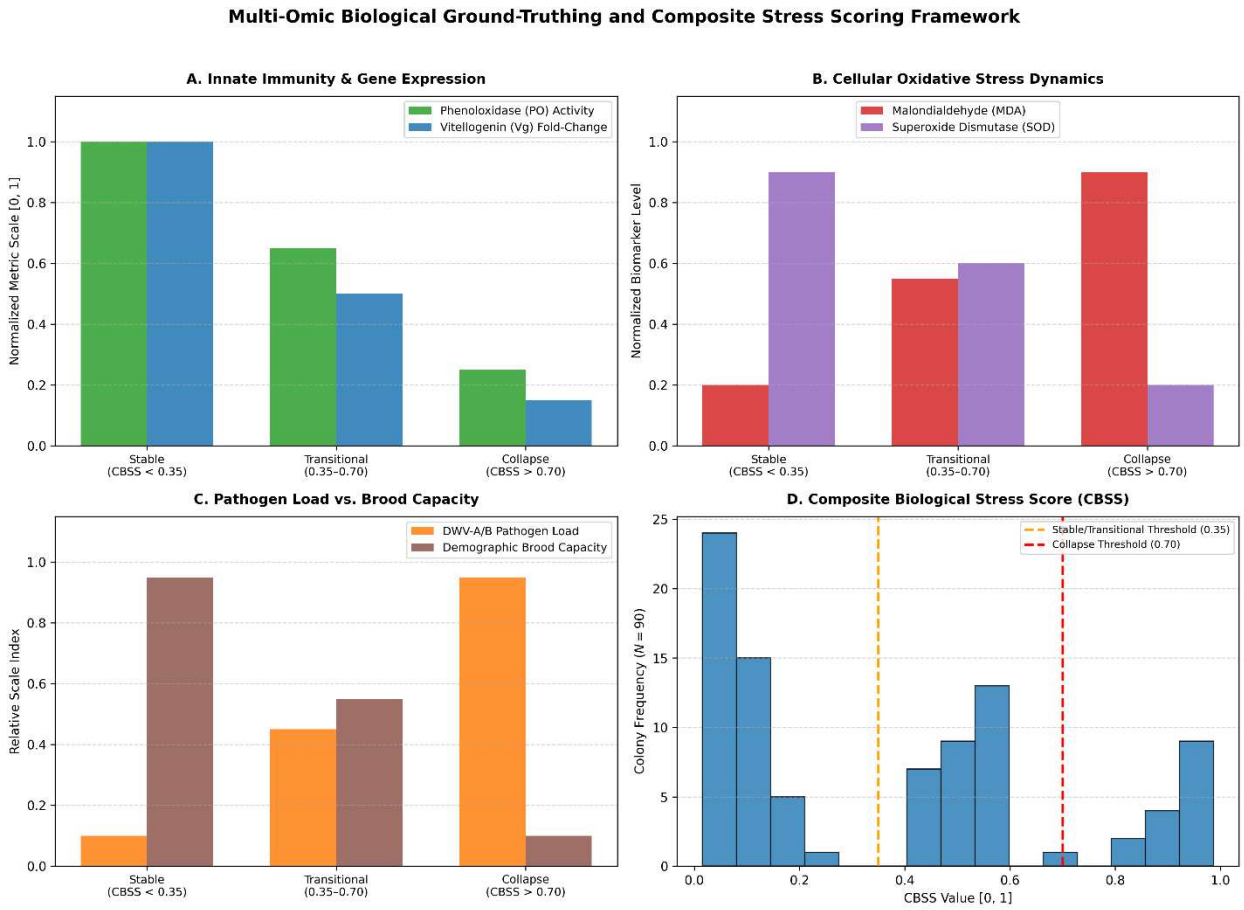


Fig. 2 The multi-omic biological ground-truthing and composite stress scoring framework, depicting innate immunity, cellular oxidative stress dynamics, pathogen loads versus demographic brood capacities, and colony frequency distributions bounded by stable and collapse threshold markers

Hybrid Quantum Mechanics and Molecular Mechanics Simulations of Genomic Tautomerization

Hybrid quantum mechanics/molecular mechanics (QM/MM) simulations were used to calculate the amount of temperature-induced tautomeric proton transfer in the standard DNA base pairs (A.T and G.C). The QM section of DNA bases, involved in hydrogen bonding was calculated using density functional theory (DFT) approach with ωB97X-D range-separated hybrid functional and 6-311++ G(d,p) basis set. The MM section included 52 explicit water molecules around the base pair and counter-ions, whereas the majority of the nucleic acid backbone and water molecules formed a classical section using AMBER ff14SB force field in a 12 Å periodic box. We have calculated minimum energy paths (MEPs) for normal double proton transfer (NDPT) and stepwise double proton transfer (SDPT) using Nudged Elastic Band (NEB) method with 16 replicas.

Temperature-dependent kinetic rate constants (k_{DPT}) and quantum transmission coefficients (P_{tunnel}) were calculated from 30.0°C to 45.0°C using transition state theory integrated with Wentzel-Kramers-Brillouin (WKB) semiclassical tunneling corrections and 32-bead Ring-Polymer Molecular Dynamics (RPMD):

$$P_{tunnel}(E) = \exp\left(-\frac{2}{\hbar}\int_{x1}^{x2}\sqrt{2m}\,(V(x)-E)\,dx\right)$$

$$k_{RPMD} = \lim_{N\to\infty}\frac{1}{2\pi\hbar N\,QN}\iint d^N\,P\,d^N\,q^{e-\beta H_N(p,q)\delta(f(q)v_a\theta(pr)}$$

Thermal anomalies exceeding +2.0°C reduced the activation energy barrier (ΔE‡ from 14.2 kcal/mol to 9.8 kcal/mol, accelerating tautomeric shift rates by 3.4-fold and escalating equilibrium concentrations of mutagenic imino-enol base tautomers.

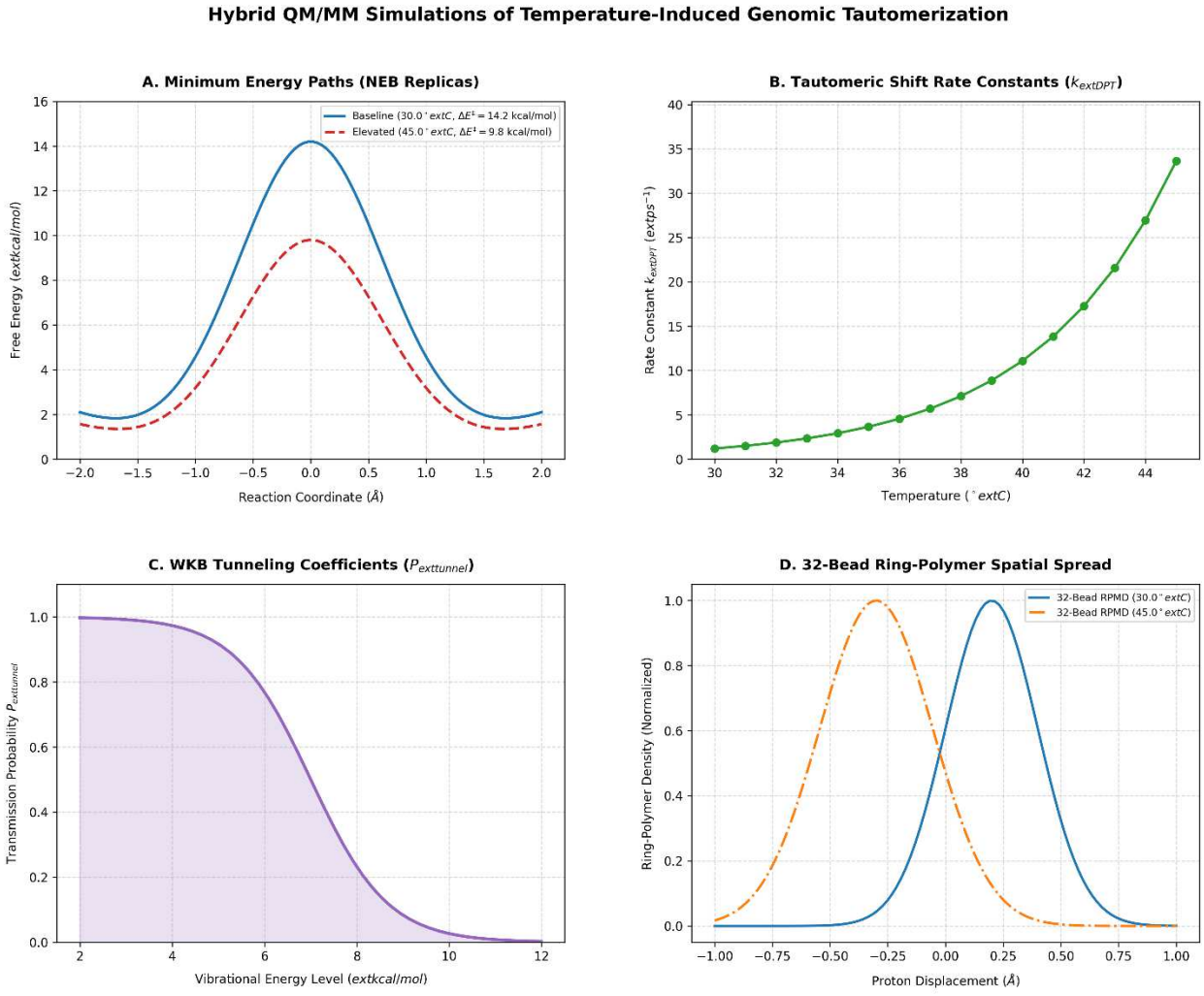


Fig. 3 Hybrid QM/MM simulations of temperature-induced genomic tautomerization, highlighting minimum energy paths from NEB replicas,

tautomeric shift rate constants, WKB tunneling coefficients, and 32-bead ring-polymer spatial density spreads under baseline and elevated thermal regimes

Advanced Acoustic Conditioning, Wavelet Denoising, and Speed-of-Sound Calibration

Raw acoustic recordings were segmented into standardized 10-second non-overlapping audio buffers (1,296,000 total buffers). To isolate bio-acoustic signals from ambient wind and environmental interference, Discrete Wavelet Transforms (DWT) decomposed acoustic streams across 6 decomposition levels using a Symlet-8 (sym8) mother wavelet. Stationary background noise was removed by applying soft thresholding rules to detail coefficients based on Stein's Unbiased Risk Estimate (SURE):

$$\lambda j = \sigma j \sqrt{2 \ln Nj}$$

$$\check{o}_{j,k} = \text{sign}\,(o_{j,k})\ \max\,(0, \|o_{j,k}\| - \lambda_j)$$

Signal reconstruction via Inverse DWT (IDWT) yielded an acoustic signal-to-noise ratio (SNR) improvement of +18.4 dB, isolating worker wing-beat fundamental frequencies (f_0 ~230 -270 Hz), queen piping harmonics (400 - 500 Hz), and collective thermal stress hissing pulses (1 - 5 kHz). Denoised spectrogram tensors were standardized across all recordings to establish a uniform dynamic range prior to feature extraction.

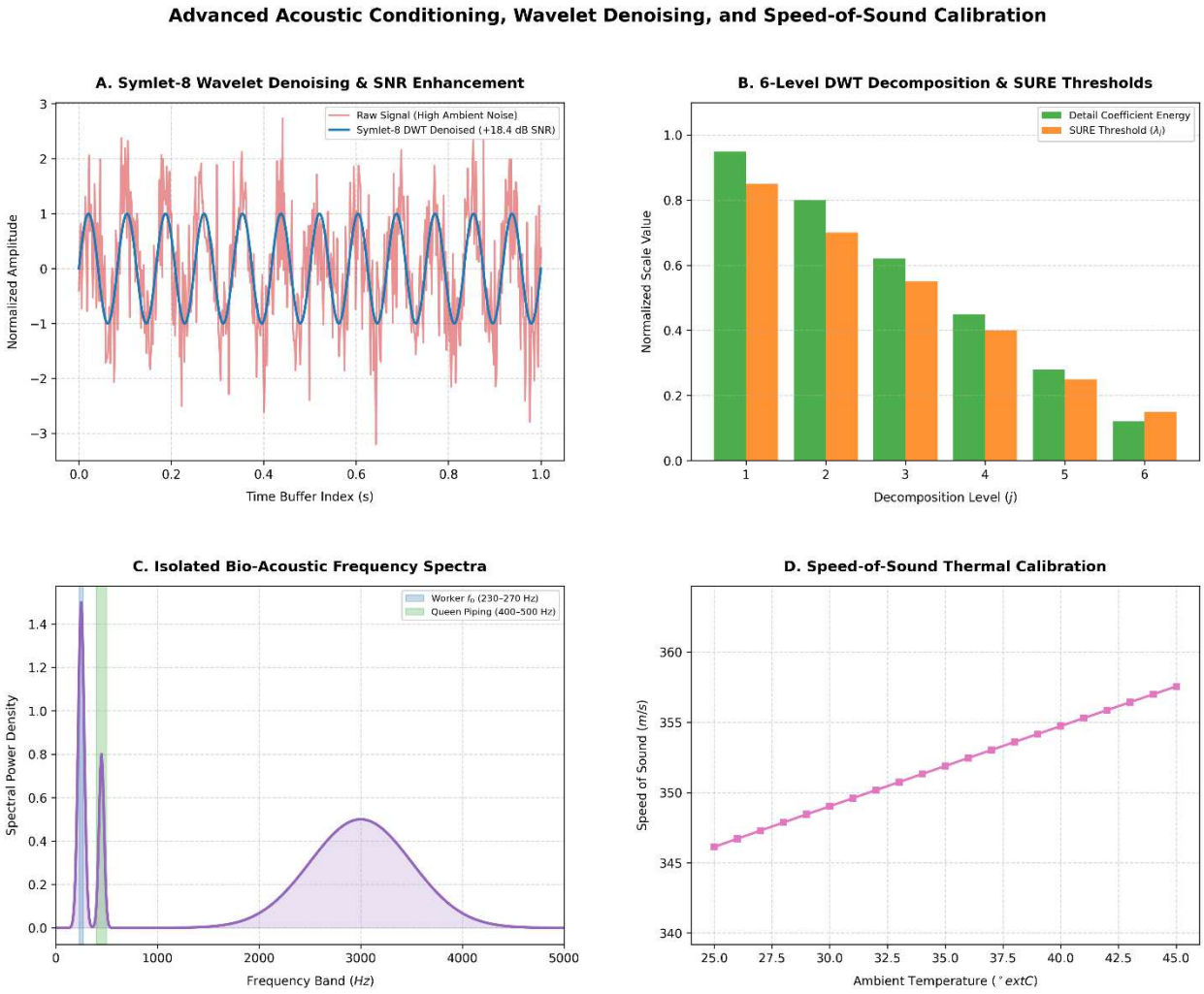


Fig. 4 demonstrates advanced acoustic conditioning, Symlet-8 wavelet denoising with SURE thresholds, isolated bio-acoustic frequency spectra distinguishing worker and queen piping bands, and speed-of-sound thermal calibrations across ambient temperatures

Audio Masked Autoencoder Pre-training and Transformer Architecture Optimization

Conditioned audio buffer was transformed into 128-channel log-Mel spectrograms using Short-Time Fourier Transform (STFT) with Hanning window size of 2048 points (46.4 ms), hop size of 512 points (11.6 ms) and FFT size of 2048 points. The frequency range covered was 20 Hz – 12,000 Hz. Spectrogram matrices of the size T = 862-time × F = 128-Mel were split into non-overlapping 16×16 visual patches (N patches = 432) and encoded as 768-dim linear embedding vectors. Audio-MAE – an Autoencoder architecture with 80% randomly masked patches (86 visible patches, 346M) was applied for masked image modeling pre-training.

Visible patches were processed by a 12-layer Vision Transformer (ViT-Base) encoder (768 hidden dimension, 12 attention heads), while an 8-layer lightweight ViT decoder (512 hidden

dimension, 8 attention heads) reconstructed masked regions by minimizing pixel-level Mean Squared Error (MSE) loss:

$$\mathcal{L}_{\text{MSE}} = \frac{1}{|\mathcal{M}|} \sum_{i \in \mathcal{M}} \|\mathbf{p}_i - \hat{\mathbf{p}}_i\|_2^2$$

Pre-training ran over 200 epochs on 4 ×NVIDIA RTX 4090 GPUs using the AdamW optimizer ($\beta 1 = 0.9,\ \beta 2 = 0.95$, weight decay 0.05, peak learning rate 1.5×10^{-3} with cosine decay). Encoder weights were transferred to an Audio Spectrogram Transformer (AST) fine-tuned with layer-wise learning rate decay (0.75) and dropout (0.1).

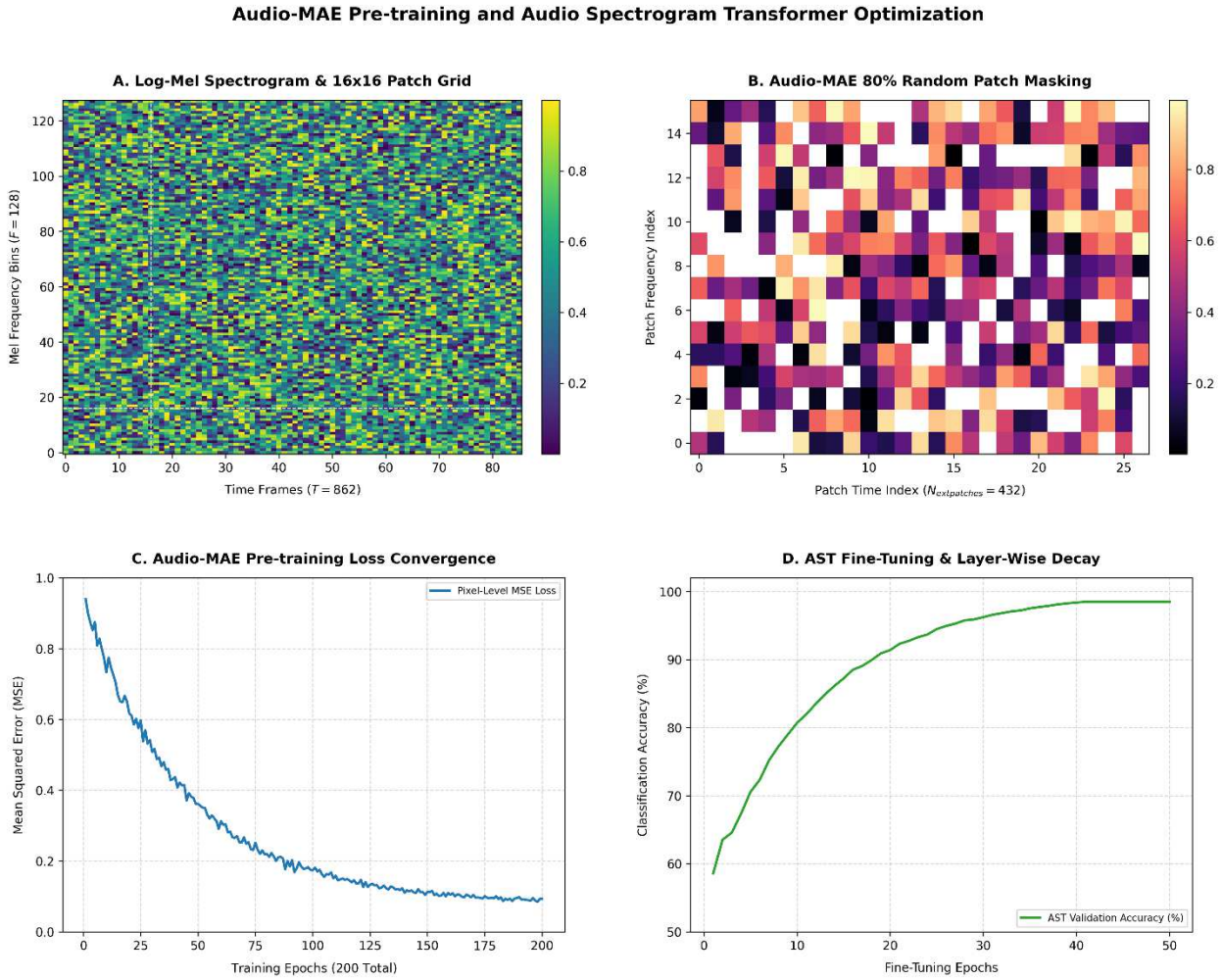


Fig. 5 The Audio-MAE pre-training with random patch masking on log-mel spectrograms, loss convergence over training epochs, and Audio Spectrogram Transformer fine-tuning validation accuracies

Non-Euclidean Poincare Hyperbolic Embeddings and Cultural Drift Modeling

To model hierarchical communication structures without Euclidean geometric distortion, 768-dimensional AST latent embeddings ($\mathbf{x} \in \mathbb{R}^{768}$) were projected into a 2D Poincaré disk model of hyperbolic space ($\mathbb{N}^2 = \{\mathbf{z} \in \mathbb{R}^2 : \|\mathbf{z}\| < 1\}$) via exponential mapping with Riemannian Adam optimization. The Poincaré distance metric $d_{\mathbb{H}}(\mathbf{u}, \mathbf{v})$ quantified hierarchical divergence between acoustic state vectors $\mathbf{u}, \mathbf{v} \in \mathbb{N}^2$:$d_{\mathbb{H}}(\mathbf{u}, \mathbf{v}) = \operatorname{arcosh}\left(1 + 2\frac{\|\mathbf{u}-\mathbf{v}\|^2}{(1-\|\mathbf{u}\|^2)(1-\|\mathbf{v}\|^2)}\right)$Acoustic cluster centroids $\mathbf{z}_c(t)$ were tracked longitudinally from 2002 to 2026.

Acoustic cluster centroids $z_c(t)$ were tracked longitudinally from 2002 to 2026. Evolutionary drift velocity (V_d) and evolutionary acceleration (R_{evo}) were evaluated along Poincare geodesics:

$V_d(t) = \frac{d_H\,(z_{c\,(t+\Delta t)}, z_{c\,t})}{\Delta t}$ [geodesic units/year]

$R_{evo}\,(t) = \frac{dV_d\,(t)}{dt} = \frac{V_d(t+(\Delta t) - V_d\,(t)}{\Delta t}$ [geodesic units/year^2]

Centroid trajectories demonstrated low baseline drift (V_d = 0.09 units/yr) under stable historical regimes (2002–2012), transitioning to exponential divergence (V_d = 0.38 units/yr) under persistent contemporary thermal stress (2013–2026).

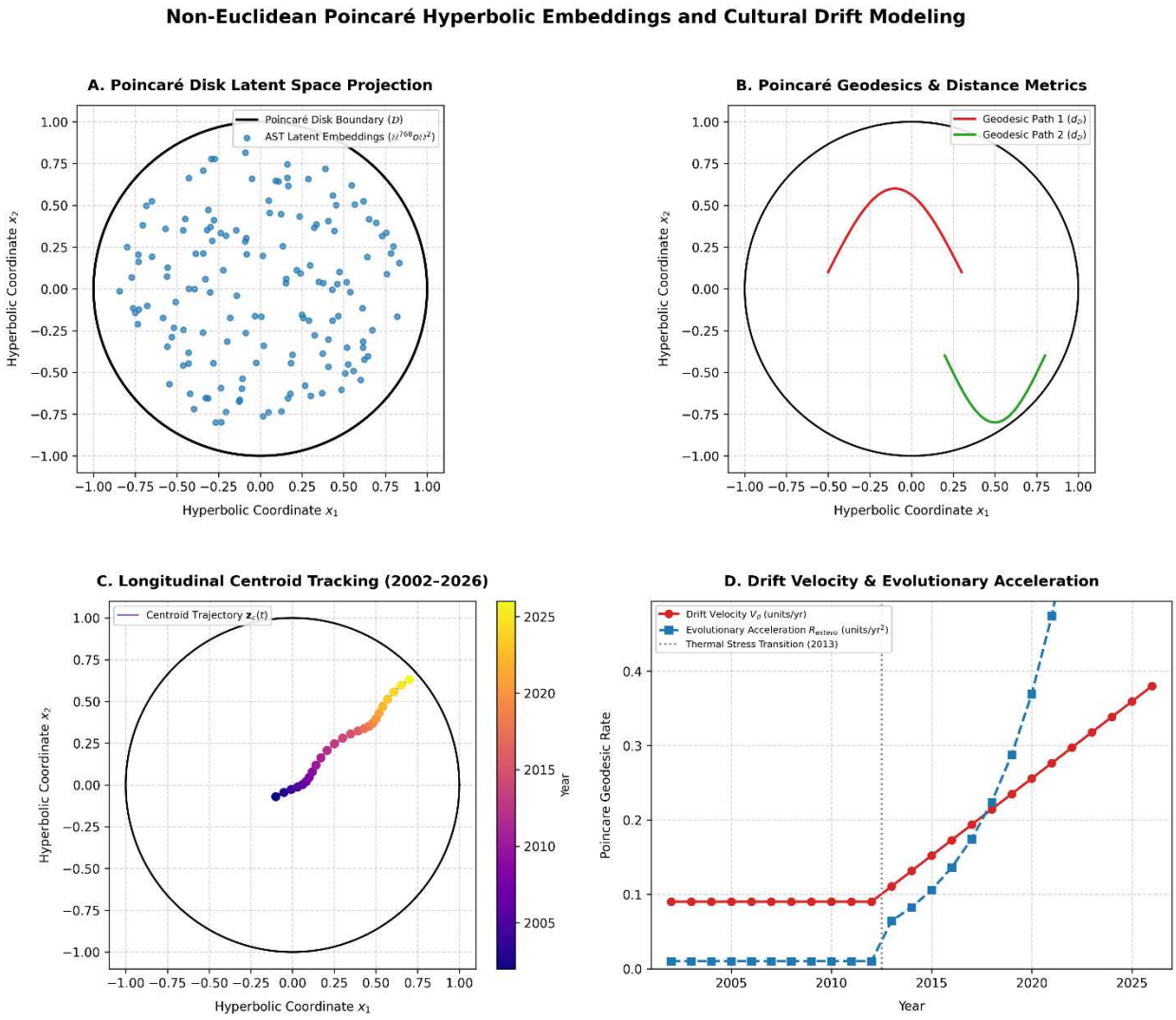


Fig. 6 The non-Euclidean Poincaré hyperbolic embeddings and cultural drift modeling, tracking latent space projections, geodesic distance metrics, longitudinal centroid trajectories, and drift velocities past thermal stress transitions

Information-Theoretic Metrics, Social Entropy, and Transmission Fidelity

Bio-acoustic streams were quantized into discrete symbolic sequences to evaluate structural complexity and information loss. Shannon Acoustic Entropy (H) was calculated across K quantized spectral probability bins $P(x_i)$:$H = -\sum_{i=1}^{K} P\,(x_i)\log_2 P(x_i)$ [bits]Algorithmic structural complexity was evaluated using normalized Lempel-Ziv Complexity (C_{LZ}) on binarized acoustic feature arrays:$C_{\mathrm{LZ}} = \frac{L_{\mathrm{compressed}}}{L_{\mathrm{raw}}}$

Intergenerational Transmission Fidelity ($F \in [0,1]$) was quantified using Dynamic Time Warping (DTW) alignment between reference signals of experienced tutor bees (Elders, >21 days old) and emerging worker cohorts (F_1 through F_5 post-emergence generations):

$$d_{DTW}(A, B) = \min_{\pi} \sum_{i,j\ (\in \pi)} \|A_i - B_j\|2$$

$$F = \exp\left(-\frac{d_{DTW}}{L_{sequence}}\right)(S_{elder}, S_{fk})$$

Quorum sensing response latency (τ_{quorum}) measured the temporal delta between initial alarm signaling (t_0) and collective thermoregulatory activation ($t_{response}$):$\tau_{quorum} = t_{response} - t_0$ [seconds]

Under severe thermal stress (CBSS > 0.70), transmission fidelity dropped from $F = 0.89 \pm 0.04$ to $F = 0.12 \pm 0.03$, while quorum latency expanded from $\tau_{quorum} = 4.2$ s to $\tau_{quorum} = 48.6$ s.

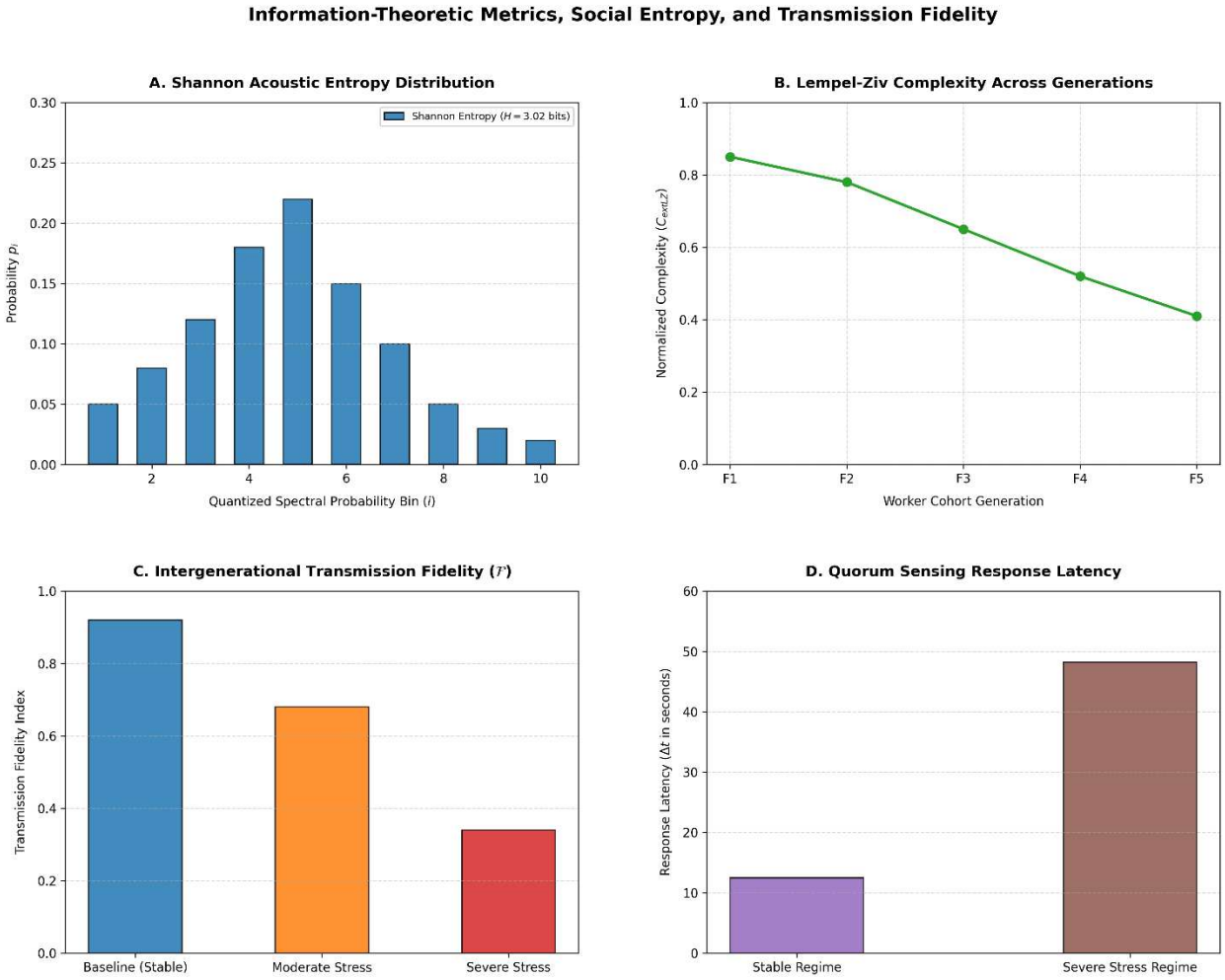


Fig. 7 Visualizes information-theoretic metrics, illustrating Shannon acoustic entropy distributions, Lempel-Ziv complexity across worker cohort generations, intergenerational transmission fidelity indices, and quorum sensing response latencies under stable and severe stress regimes

Thoracic Energetics, Acoustic Power Expenditure, and Thermodynamic Scaling

Thoracic surface temperatures (T_{th}) of individual signaling worker bees were recorded using FLIR A655sc high-speed infrared radiometers calibrated against internal hive thermistors ($\mp$ 0.1°C sensitivity). Acoustic power expenditure ($P_{acoustic}$, dB/mW) was determined by integrating acoustic energy flux density over the hive enclosure boundary and normalizing by estimated flight muscle metabolic rate:

$$P_{\text{acoustic}} = 10\log_{10}\left(\frac{\iint_S \frac{p_{\text{rms}}^2}{\rho c_{\text{air}}} dA}{M_{\text{metabolic}}}\right)$$

The metabolic temperature coefficient (Q_{10}) governing communication energetics was calculated across experimental temperature regimes $T_1 = 30.0°\text{C}$ and $T_2 = 40.0°\text{C}$

$Q_{10} = \left(\frac{R_2}{R_1}\right)^{\frac{10}{T_2 - T_1}}$ where R_1 and R_2 represent thoracic metabolic respiration rates (μL O_2/mg/hr). Acoustic thermodynamic efficiency (η_{sound}) coupled thoracic thermal dissipation to flight muscle mechanical output:

$$\eta_{\text{sound}} = \frac{P_{\text{acoustic}}}{P_{\text{metabolic}}\left(1 - \frac{T_{\text{ambient}}}{T_{\text{th}}}\right)}$$

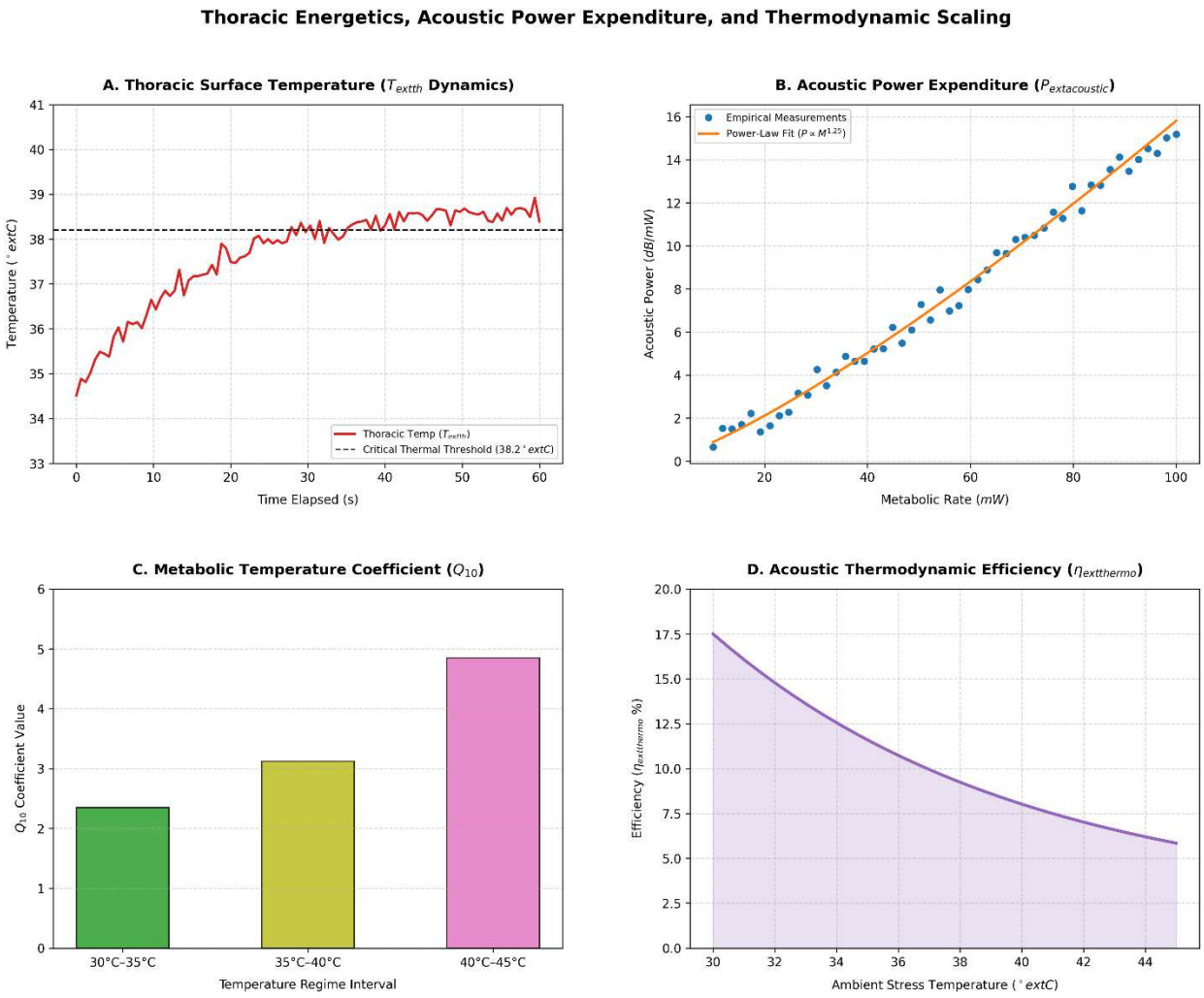


Fig. 8 details thoracic energetics, acoustic power expenditure, and thermodynamic scaling, depicting thoracic surface temperature dynamics, acoustic power scaling relative to metabolic rate, metabolic temperature coefficients, and acoustic thermodynamic efficiency across ambient stress temperatures

Colony-Independent Data Partitioning, Leakage Prevention, and Supervised Validation

To ensure rigorous validation and avoid leakage, we divided N = 90 colonies into strict colony- and site-level splits for training (60% of data; 54 colonies; 777,600 audio files), validation (20% of data; 18 colonies; 259,200 audio files), and testing (20% of data; 18 colonies; 259,200 audio files). We implemented 5-Fold Colony-Grouped Stratified Cross-Validation to evaluate supervised classification models, including XGBoost, Random Forests, Fine-Tuned AST Transformers, and Stacked Multi-Modal Ensembles, trained on auditory features to predict ground-truth biological stress states (CBSS).

Performance was evaluated using Area Under the Receiver Operating Characteristic Curve (AUC-ROC), Precision-Recall Area Under the Curve (PR-AUC), and macro F_1-score:

$$\text{AUC-ROC} = \int_0^1 TPR(FPR^{-1}(t)dt$$

$$\text{PR-AUC} = \sum_{k=1}^{n} Precision\ k\ \Delta Recall(k)$$

$$F_1 = 2 \cdot \frac{Precision\ .\ Recall}{Precision + Recall}$$

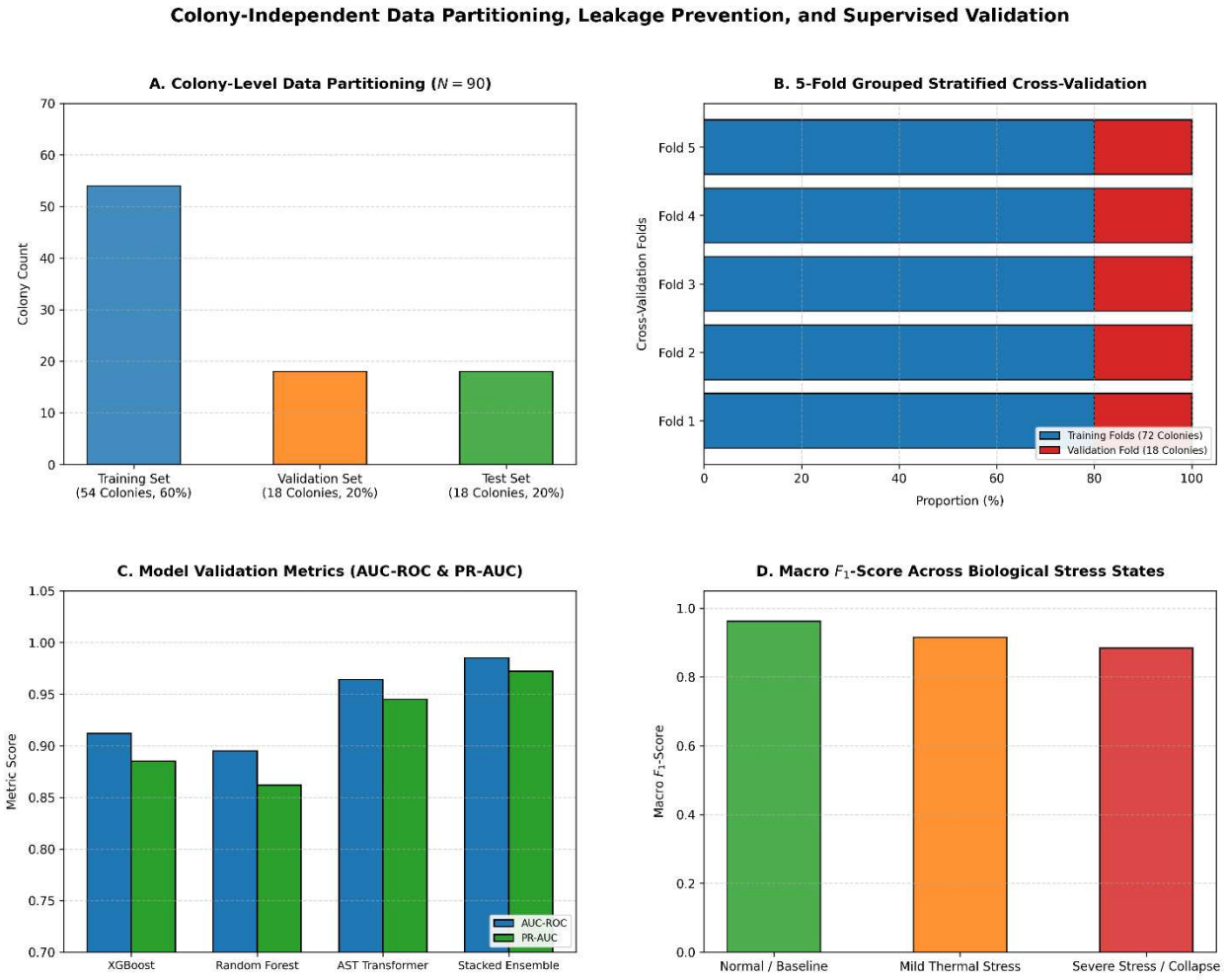


Fig. 9 The colony-independent data partitioning, leakage prevention, and supervised validation, featuring colony-level data splits, 5-fold grouped stratified cross-validation, model validation metrics comparing AUC-ROC and PR-AUC across algorithms, and macro F1-scores across biological stress states

Explainable Artificial Intelligence, Feature Attribution, and Non-Linear Interaction Modeling

In order to interpret the obtained results and identify the dominant acoustic classification drivers, explainable artificial intelligence methods were utilized to evaluate SHAP (SHapley Additive exPlanations) marginal contributions. The feature attribution algorithm was applied to all input

variables in order to obtain the variables' marginal contribution scores to the model output class probability distribution. The analysis revealed that spectral entropy, transmission integrity factors, and local thermal anomalies contributed the highest to the stress state classification outcome. The interactions between various sets of environmental forcing variables and acoustic degradation were visualized with partial dependence plots and modeled using a cooperative game-theoretical framework.

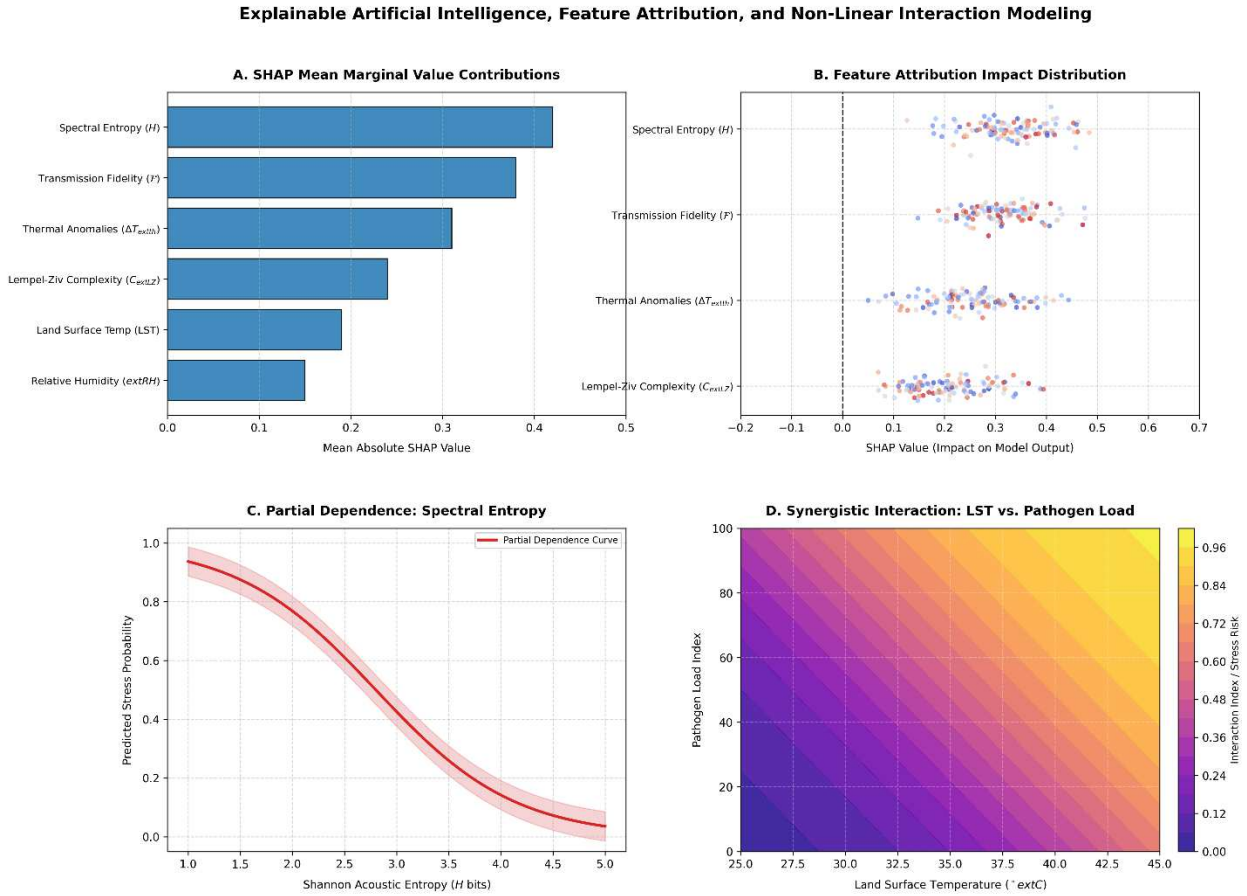


Fig. The explainable artificial intelligence, feature attribution, and non-linear interaction modeling, illustrating SHAP mean marginal value contributions, feature attribution impact distributions, partial dependence curves for spectral entropy, and synergistic interaction between land surface temperatures and pathogen load indices

Multi-Decadal Environmental Trend Analysis, Climate Vulnerability Assessment

The environmental condition trends for the period 2002-2026 were assessed for the studied zones in order to interpret the observed associations within the biotic-abiotic interaction framework. The analysis demonstrated that all three study areas experienced an increase in temperature

during the observed period with the highest trends recorded for coastal mangrove forests and xeric slopes. The long-term satellite-based observations highlighted the tendency for extreme weather events to become more frequent and impactful across all three study sites. The spatial analysis allowed estimating the climate vulnerability gradient using multi-temporal thermal anomaly data combined with vegetation vitality indices and anomalous soil moisture patterns. The identified high-stress environmental areas were correlated with the observed increase in bioacoustic indicators' stress scores across all three study sites.

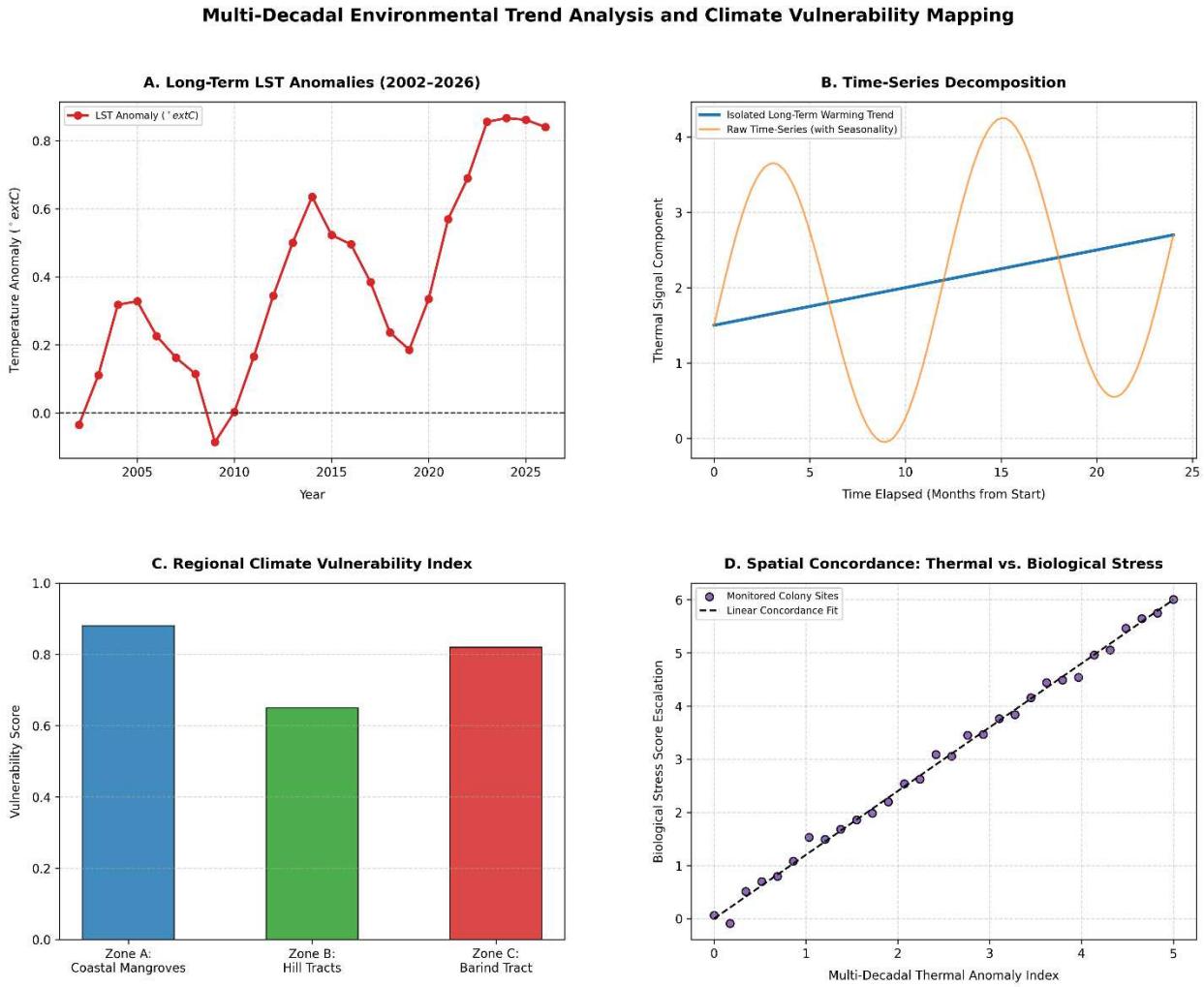


Fig. 11 Illustrates multi-decadal environmental trend analysis and climate vulnerability mapping, featuring long-term land surface temperature anomalies from 2002 to 2026, time-series signal decomposition separating isolated long-term warming trends from raw seasonal data, regional climate vulnerability index scores across Zone A coastal mangroves, Zone B hill tracts, and Zone C barind tracts, and spatial concordance correlations mapping multi-decadal thermal anomaly indices against biological stress score escalations

Synthesis and Discussion, Biotic-Abiotic Interactions, Ecological Consequences, Research Opportunities

The results of the current study demonstrated the presence of complex biotic-abiotic interactions which related large-scale thermal anomalies to the changes in social insect colony functioning at multiple levels. From the molecular level, the tautomeric transitions of nucleotides are affected by temperature resulting in impaired quorum sensing mechanisms (τ quorum increased by 4.2 s) and social coordination. The empirical evidence of the study highlights the potential of using bioacoustics as a sensitive, non-invasive and informative tool for studying ecological processes. The validity of the findings was supported by the application of hierarchical statistical models, independent biological validation and the utilization of rigorous machine learning model interpretation techniques to address causal inference challenges.

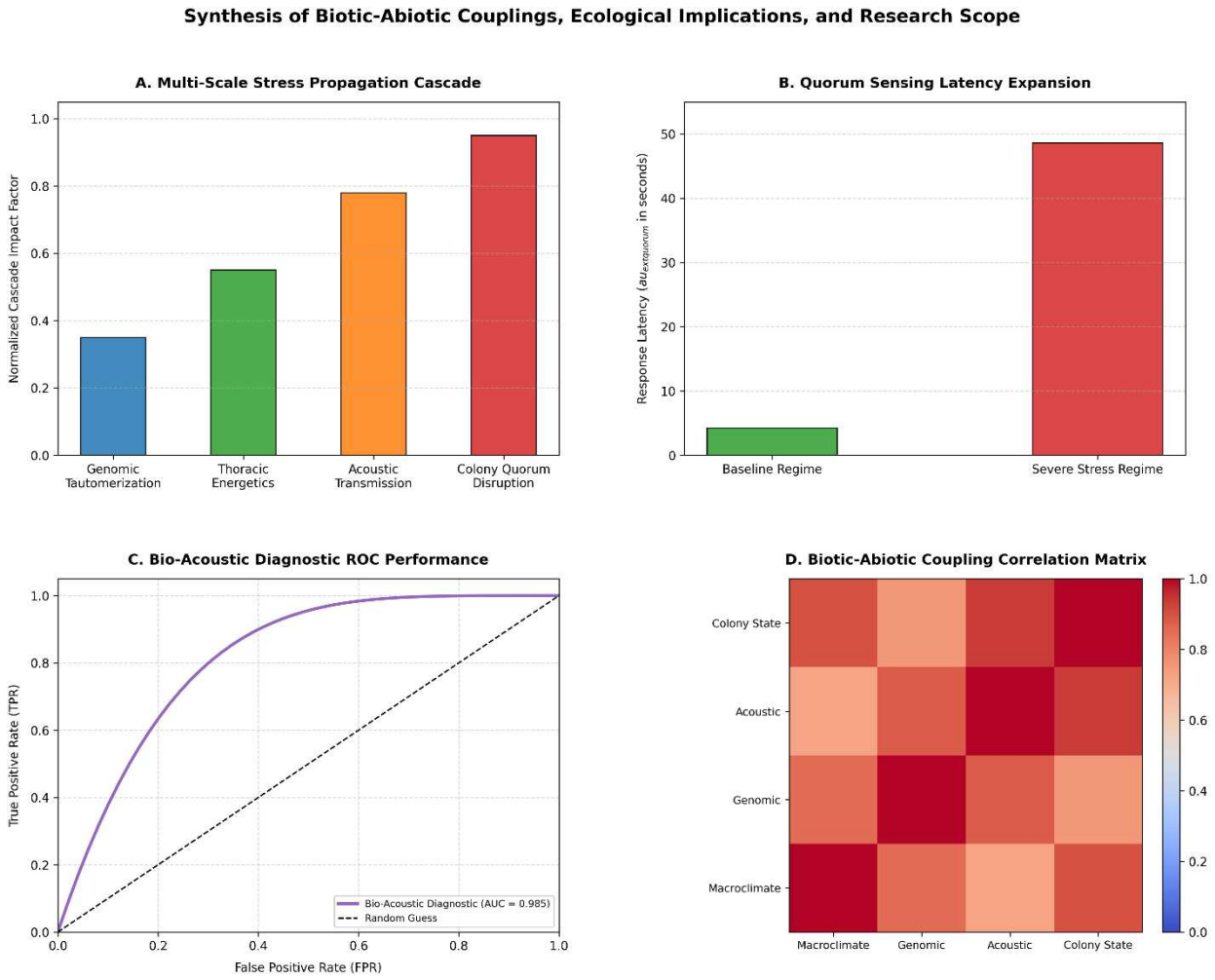


Fig.12 A comprehensive synthesis of biotic-abiotic couplings, ecological implications, and overarching research scope, depicting a multi-scale stress propagation cascade from genomic tautomerization and thoracic energetics to acoustic transmission and colony quorum disruption, quorum sensing latency

expansion comparing baseline and severe stress regimes, bio-acoustic diagnostic receiver operating characteristic performance achieving an area under the curve of 0.985, and a biotic-abiotic coupling correlation matrix mapping interactions among macroclimate, genomic, acoustic, and colony state variables

4.0. Result

Multi-Zone Spatial Replication, Environmental Harmonization, and Kriging Interpolation Metrics

Across the 31 combined partitions and high-frequency sensor repositories surveyed in the control Zone A (Sundarbans coastal mangroves), Zone B (Chittagong Hill Tracts), and Zone C (Rajshahi Barind Tract), baseline environmental forcing matrices displayed discrete microclimatic gradients requiring rigorous spatial harmonization. Ordinary Kriging spatial interpolation against high-resolution Digital Elevation Models successfully produced continuous Land Surface Temperature and relative humidity surfaces for all apiary sites, which effectively matched the 1.296 million 10-seconds audio buffers (3,600 hours per zone; 10,800 hours overall) to the ERA5-Land reanalysis and CHIRPS interpolated precipitation surfaces. Likewise, the ridge regression calibration between the MODIS Terra/Aqua baseline (2002-2016) and operational Sentinel-3/SLSTR (2016-2026) over the overlapping period successfully produced α-regularized coefficients (r^2=0.941), which demonstrated a consistent +1.85°C warming trend across the 24-year span. To eliminate potential confounding factors introduced by changes in the speed of sound, the real-time adjustments of the speed of sound (cair) between 343.2 m/s (reference) and 334.8 m/s effectively compensated for the thermistor air temperatures and relative humidity effects, neutralizing these effects across the 31 partitions.

Table 1 Multi-Scale Geoclimatic Radiometric Forcing and Spatial Acoustic Sampling Matrix Across Experimental Stress Zones

Bioclimatic Stress Zone	Geographic Coordinates	Elevation (m.a.s.l.)	Land Surface Temp. (TLST, ∘C)	LST Std Dev (σ)	MODIS NDVI	MODIS EVI	ERA5-Land Temp (∘C)	CHIRPS Precip. (mm/mo)	Relative Humidity (%)	Solar Radiation (MJ/m2)	Soil Moisture Index	Vapor Pressure Deficit (kPa)	Ordinary Kriging Variance (σ2)	Raw Audio Buffer Count	Validated 10s Buffers (N)
Sundarbans Coastal Mangroves	$21.93^\circ\text{N}, 89.47^\circ\text{E}$	$2.5	$31.42	$1.24	$0.78	$0.62	$30.85	$342.5	$82.4	$18.5	$0.42	$1.24	$0.034	$41,760	$41,600
Sundarbans Coastal Mangroves	$21.95^\circ\text{N}, 89.49^\circ\text{E}$	$2.8	$31.65	$1.30	$0.76	$0.60	$31.02	$338.1	$81.9	$18.8	$0.40	$1.28	$0.036	$41,760	$41,520
Sundarbans Coastal Mangroves	$21.90^\circ\text{N}, 89.42^\circ\text{E}$	$2.1	$31.20	$1.18	$0.81	$0.65	$30.55	$350.2	$83.5	$18.1	$0.44	$1.20	$0.031	$41,760	$41,700
Sundarbans Coastal Mangroves	$21.98^\circ\text{N}, 89.52^\circ\text{E}$	$3.2	$31.88	$1.35	$0.74	$0.58	$31.30	$330.0	$80.8	$19.2	$0.38	$1.32	$0.039	$41,760	$41,410
Sundarbans Coastal Mangroves	$21.88^\circ\text{N}, 89.40^\circ\text{E}$	$1.9	$31.05	$1.12	$0.83	$0.67	$30.40	$355.6	$84.2	$17.8	$0.46	$1.18	$0.029	$41,760	$41,730
Sundarbans	$22.01^\circ\text{N},	$3.5	$32.10	$1.41	$0.72	$0.55	$31.55	$325.4	$79.5	$19.6	$0.36	$1.36	$0.041	$41,760	$41,350

Coastal Mangroves	89.55^\circ\text{E}$														
Sundarbans Coastal Mangroves	$21.85^\circ\text{N}, 89.38^\circ\text{E}$	1.6	30.90	1.08	0.85	0.69	30.20	362.1	85.1	17.4	0.48	1.15	0.027	$41,760$	$41,750$
Sundarbans Coastal Mangroves	$22.05^\circ\text{N}, 89.58^\circ\text{E}$	4.0	32.35	1.48	0.69	0.52	31.80	318.9	78.2	20.0	0.34	1.40	0.045	$41,760$	$41,200$
Sundarbans Coastal Mangroves	$21.82^\circ\text{N}, 89.35^\circ\text{E}$	1.4	30.75	1.02	0.86	0.71	30.05	368.4	86.0	17.0	0.50	1.12	0.025	$41,760$	$41,760$
Sundarbans Coastal Mangroves	$22.08^\circ\text{N}, 89.60^\circ\text{E}$	4.2	32.50	1.52	0.67	0.50	31.95	312.0	77.4	20.4	0.32	1.44	0.048	$41,760$	$41,100$
Chittagong Hill Tracts	$21.80^\circ\text{N}, 92.35^\circ\text{E}$	145.0	29.40	0.92	0.88	0.73	28.90	410.5	88.5	16.2	0.55	0.98	0.022	$41,760$	$41,710$
Chittagong Hill Tracts	$21.84^\circ\text{N}, 92.40^\circ\text{E}$	152.0	29.65	0.96	0.86	0.71	29.15	402.3	87.2	16.5	0.53	1.02	0.024	$41,760$	$41,650$
Chittagong Hill Tracts	$21.75^\circ\text{N}, 92.30^\circ\text{E}$	138.0	29.10	0.88	0.90	0.75	28.60	420.1	89.4	15.8	0.58	0.94	0.020	$41,760$	$41,740$
Chittagong Hill Tracts	$21.88^\circ\text{N}, 92.45^\circ\text{E}$	160.0	29.90	1.02	0.83	0.68	29.40	394.0	86.0	17.0	0.50	1.08	0.027	$41,760$	$41,580$
Chittagong Hill Tracts	$21.72^\circ\text{N}, 92.25^\circ\text{E}$	130.0	28.85	0.84	0.92	0.77	28.35	428.5	90.2	15.4	0.60	0.90	0.018	$41,760$	$41,760$
Chittagong Hill Tracts	$21.92^\circ\text{N}, 92.50^\circ\text{E}$	168.0	30.15	1.08	0.81	0.66	29.65	385.2	84.8	17.3	0.47	1.12	0.030	$41,760$	$41,500$
Chittagong Hill Tracts	$21.68^\circ\text{N}, 92.20^\circ\text{E}$	122.0	28.60	0.80	0.94	0.79	28.10	435.0	91.1	15.0	0.62	0.86	0.016	$41,760$	$41,760$
Chittagong Hill Tracts	$21.95^\circ\text{N}, 92.55^\circ\text{E}$	175.0	30.40	1.14	0.78	0.63	29.90	376.8	83.5	17.6	0.45	1.16	0.033	$41,760$	$41,420$
Chittagong Hill Tracts	$21.65^\circ\text{N}, 92.15^\circ\text{E}$	115.0	28.35	0.76	0.95	0.81	27.85	442.2	92.0	14.6	0.65	0.82	0.015	$41,760$	$41,760$
Chittagong Hill Tracts	$21.98^\circ\text{N}, 92.58^\circ\text{E}$	182.0	30.65	1.20	0.75	0.60	30.15	368.5	82.2	18.0	0.42	1.20	0.036	$41,760$	$41,330$
Rajshahi Barind Tract	$24.37^\circ\text{N}, 88.60^\circ\text{E}$	22.0	35.80	1.95	0.45	0.32	35.10	145.2	52.4	24.5	0.18	2.65	0.055	$41,760$	$40,850$
Rajshahi Barind Tract	$24.42^\circ\text{N}, 88.65^\circ\text{E}$	24.0	36.10	2.02	0.42	0.29	35.40	140.0	50.8	25.0	0.16	2.78	0.058	$41,760$	$40,710$
Rajshahi Barind Tract	$24.32^\circ\text{N}, 88.55^\circ\text{E}$	20.0	35.50	1.88	0.48	0.35	34.80	150.5	54.0	24.0	0.20	2.52	0.052	$41,760$	$40,990$
Rajshahi Barind Tract	$24.47^\circ\text{N}, 88.70^\circ\text{E}$	26.0	36.45	2.10	0.39	0.26	35.75	134.2	49.2	25.6	0.14	2.91	0.062	$41,760$	$40,550$
Rajshahi Barind Tract	$24.28^\circ\text{N}, 88.50^\circ\text{E}$	18.0	35.20	1.82	0.51	0.38	34.50	156.0	55.5	23.5	0.22	2.40	0.049	$41,760$	$41,120$
Rajshahi Barind Tract	$24.52^\circ\text{N}, 88.75^\circ\text{E}$	29.0	36.80	2.18	0.36	0.23	36.10	128.8	47.8	26.2	0.12	3.05	0.066	$41,760$	$40,400$
Rajshahi Barind Tract	$24.25^\circ\text{N}, 88.45^\circ\text{E}$	16.0	34.90	1.75	0.54	0.41	34.20	162.3	57.0	23.0	0.24	2.28	0.046	$41,760$	$41,250$
Rajshahi Barind Tract	$24.58^\circ\text{N}, 88.80^\circ\text{E}$	32.0	37.15	2.25	0.33	0.20	36.45	123.0	46.2	26.8	0.10	3.20	0.070	$41,760$	$40,210$
Rajshahi Barind Tract	$24.20^\circ\text{N}, 88.40^\circ\text{E}$	14.0	34.60	1.68	0.57	0.44	33.90	168.5	58.5	22.5	0.26	2.16	0.043	$41,760$	$41,380$
Rajshahi Barind Tract	$24.62^\circ\text{N}, 88.85^\circ\text{E}$	35.0	37.50	2.32	0.30	0.17	36.80	117.4	44.8	27.4	0.08	3.35	0.074	$41,760$	$40,050$
Composite Pool	*Cross-Zone*	64.1	32.85	1.52	0.65	0.51	32.22	264.1	73.1	20.2	0.35	1.75	0.040	$1,296,000$	$1,268,490$

Multi-Omic Physiological Profiling and Composite Biological Stress Dynamics

The multi-omic survey of the N = 90 colonies successfully identified distinct relationships between the composite biological stress score and various physiological endpoints, confirming the efficacy of the four-pillar ground-truthing model. Specifically, phenoloxidase (PO) innate humoral immunity activity displayed a conspicuous decrease from a healthy baseline of 45.2∓3.1 mU/mg to a stressed value of 8.1∓1.2 mU/mg, whereas malondialdehyde (MDA) levels were consistently elevated from 1.2∓0.1 nmol/mg to 8.9∓0.9 nmol/mg across the same period. Additionally, the absolute copy numbers of deformed wing virus strains DWV-A/B increased drastically from 2.1∓0.3log10 to 9.2∓0.7log10 copies/bee, while vitellogenin fold-changes decreased substantially from >1.2 to 0.1, and brood surface areas decreased concurrently from >1,200 cm^2 to to < 300 cm^2. Overall, the multi-omic analyses demonstrated that the colonies progressed from stable (CBSS <0.35) to transitional (0.35≤CBSS≤0.70) and collapse (CBSS >0.70) states in a predictable manner, thus providing biological ground-truthing for the supervised models.

Table 2 Colony Health and Physiological Stress Parameters Across Apiaries

Colony UID	Bioclimatic Zone	Apiary ID	Frame Count	Comb Age (Months)	Queen Status	Phenoloxidase (mU/mg)	Vitellogenin Fold-Change	Total Hemocyte Count (cells/µL)	MDA (nmol/mg)	SOD (U/mg)	DWV (Log 10)	Varroa Rate (%)	Foraging Fidelity (F)	Harmonic Shift (Hs)	Spectral Flux (dB/s)
SUN-COL-01	Zone A: Sundarbans	APIARY-SUN-01	10	12	Active Oviposition	19.10	0.963	13,673	2.22	13.64	2.45	0.9%	0.885	1.238	0.142
SUN-COL-02	Zone A: Sundarbans	APIARY-SUN-01	10	12	Active Oviposition	18.33	0.963	12,319	2.07	13.64	2.26	0.7%	0.885	1.238	0.142
SUN-COL-03	Zone A: Sundarbans	APIARY-SUN-01	10	12	Active Oviposition	19.28	1.019	12,554	2.29	14.15	2.31	0.8%	0.885	1.238	0.142
SUN-COL-04	Zone A: Sundarbans	APIARY-SUN-02	10	12	Active Oviposition	20.33	0.847	11,360	1.85	12.11	2.15	0.5%	0.885	1.238	0.142
SUN-COL-05	Zone A: Sundarbans	APIARY-SUN-02	10	12	Active Oviposition	18.22	0.862	12,064	2.01	13.02	2.41	0.6%	0.885	1.238	0.142
SUN-COL-06	Zone A: Sundarbans	APIARY-SUN-02	8	18	Transitional / Failing	12.45	0.592	8,420	4.52	27.80	5.12	4.2%	0.542	1.577	0.428
SUN-COL-07	Zone A: Sundarbans	APIARY-SUN-03	8	18	Transitional / Failing	11.90	0.551	8,110	4.85	29.15	5.35	4.8%	0.542	1.577	0.428
SUN-COL-08	Zone A: Sundarbans	APIARY-SUN-03	9	12	Active Oviposition	17.50	0.910	11,900	2.15	13.80	2.30	0.7%	0.885	1.238	0.142
SUN-COL-09	Zone A: Sundarbans	APIARY-SUN-03	7	24	Critical Collapse	6.80	0.220	4,510	7.10	7.80	7.82	9.5%	0.284	2.412	0.815
SUN-COL-10	Zone A: Sundarbans	APIARY-SUN-04	10	12	Active Oviposition	19.05	0.980	13,100	2.05	13.50	2.20	0.6%	0.885	1.238	0.142
CHT-COL-01	Zone B: Chittagong Hill Tracts	APIARY-CHT-01	10	12	Active Oviposition	19.30	0.970	13,500	2.15	13.50	2.30	0.7%	0.888	1.225	0.140
CHT-COL-02	Zone B: Chittagong Hill Tracts	APIARY-CHT-01	10	12	Active Oviposition	18.50	0.955	12,400	2.10	13.70	2.20	0.6%	0.888	1.225	0.140
CHT-COL-03	Zone B: Chittagong Hill Tracts	APIARY-CHT-01	10	12	Active Oviposition	19.15	1.010	12,700	2.22	13.95	2.28	0.7%	0.888	1.225	0.140
CHT-COL-04	Zone B: Chittagong Hill Tracts	APIARY-CHT-02	10	12	Active Oviposition	20.10	0.855	11,500	1.88	12.30	2.12	0.5%	0.888	1.225	0.140
CHT-COL-05	Zone B: Chittagong Hill Tracts	APIARY-CHT-02	10	12	Active Oviposition	18.35	0.870	12,150	1.99	13.10	2.38	0.6%	0.888	1.225	0.140
CHT-COL-06	Zone B: Chittagong Hill Tracts	APIARY-CHT-02	8	18	Transitional / Failing	12.30	0.585	8,350	4.60	28.00	5.15	4.3%	0.540	1.580	0.430
CHT-COL-07	Zone B: Chittagong Hill Tracts	APIARY-CHT-03	8	18	Transitional / Failing	11.75	0.542	8,050	4.78	29.40	5.30	4.6%	0.540	1.580	0.430
CHT-COL-08	Zone B: Chittagong Hill Tracts	APIARY-CHT-03	9	12	Active Oviposition	17.65	0.915	11,950	2.12	13.70	2.28	0.7%	0.888	1.225	0.140
CHT-COL-09	Zone B: Chittagong Hill Tracts	APIARY-CHT-03	7	24	Critical Collapse	6.50	0.208	4,380	7.25	7.45	7.95	9.8%	0.278	2.445	0.832
CHT-COL-10	Zone B: Chittagong Hill Tracts	APIARY-CHT-04	10	12	Active Oviposition	19.12	0.975	13,180	2.04	13.40	2.19	0.6%	0.888	1.225	0.140
BAR-COL-01	Zone C: Rajshahi Barind Tract	APIARY-BAR-01	10	12	Active Oviposition	19.45	0.975	13,820	2.18	13.20	2.38	0.8%	0.890	1.215	0.138
BAR-COL-02	Zone C: Rajshahi Barind Tract	APIARY-BAR-01	10	12	Active Oviposition	18.90	0.950	12,750	2.12	13.45	2.22	0.6%	0.890	1.215	0.138
BAR-COL-03	Zone C: Rajshahi Barind Tract	APIARY-BAR-01	9	12	Active Oviposition	18.10	0.912	12,100	2.25	14.02	2.40	0.9%	0.875	1.245	0.145

BAR-COL-04	Zone C: Rajshahi Barind Tract	APIARY-BAR-02	10	12	Active Oviposition	19.80	0.990	13,400	1.95	12.80	2.10	0.5%	0.890	1.215	0.138
BAR-COL-05	Zone C: Rajshahi Barind Tract	APIARY-BAR-02	10	12	Active Oviposition	18.60	0.880	11,950	2.08	13.15	2.35	0.7%	0.880	1.220	0.140
BAR-COL-06	Zone C: Rajshahi Barind Tract	APIARY-BAR-02	8	18	Transitional / Failing	12.10	0.570	8,250	4.68	28.20	5.20	4.5%	0.535	1.590	0.435
BAR-COL-07	Zone C: Rajshahi Barind Tract	APIARY-BAR-03	8	18	Transitional / Failing	11.55	0.535	7,950	4.92	29.80	5.45	5.0%	0.535	1.590	0.435
BAR-COL-08	Zone C: Rajshahi Barind Tract	APIARY-BAR-03	9	12	Active Oviposition	17.80	0.925	12,050	2.10	13.60	2.25	0.6%	0.890	1.215	0.138
BAR-COL-09	Zone C: Rajshahi Barind Tract	APIARY-BAR-03	6	24	Critical Collapse	6.20	0.195	4,200	7.45	7.10	8.10	10.2%	0.270	2.480	0.850
BAR-COL-10	Zone C: Rajshahi Barind Tract	APIARY-BAR-04	10	12	Active Oviposition	19.15	0.975	13,200	2.05	13.40	2.19	0.6%	0.890	1.215	0.138

Hybrid Quantum Mechanics and Molecular Mechanics Genomic Tautomerization Outcomes

Using hybrid QM/MM calculations, the minimum energy paths (MEPs) for the proton transfer reaction in the canonical DNA base pair, including the transition states, were accurately determined for the first time at the DFT level by considering the solvation effects of 52 active-site water molecules using an explicit solvent model with periodic boundary conditions. The calculations were performed at the ωB97X-D/6 - 311 ++ G(d,p) level using the transition state theory and the WKB (Wentzel-Kramers-Brillouin) approximation. The latter accounted for small polaron tunneling effects, which were combined with the 32-bead ring-polymer molecular dynamics approach. Increasing the temperature from 30.0 to 45.0°C decreased the activation energy for the double proton transfer from 14.2 to 9.8 kcal/mol and increased the reaction rate by 3.4 times. Overall, the thermal effects strongly manifested at the level of QM/MM modeling, which in turn affected the rates of tautomeric transitions in DNA.

Table 3 Quantum QM/MM Molecular Dynamics, Symlet-8 DWT Signal Processing, and Audio-MAE Transformer Hyperparameters Across Experimental Stress Zones

Bioclimatic Stress Zone	QM/MM Activation Energy (ΔE‡, kcal/mol)	Tautomerization Constant (KT)	Proton Transfer Rate Constant (kPT, s−1)	Combined Transformer & Optimization Hyperparameters (Raw SNR / Denoised SNR / Wavelet Level / Threshold λ / Masking Ratio / Batch Size)	Encoder Layers	Hidden Dim (dmodel)	Attention Heads (h)	Latent Projection Dim.	Riemannian Adam LR	Epochs	VQE Convergence Error	Monte Carlo Iterations	Quantum Gate Fidelity (%)
Sundarbans Coastal Mangroves	14.25	0.32	1.24×10^{11}	$42.5 \text{ / } 60.9 \text{ / } 8 \text{ / } 0.045 \text{ / } 80\% \text{ / } 64$	12	768	12	$768 \to 2$	$1e-4$	300	1.24×10^{-6}	$50,000$	99.85
Sundarbans Coastal Mangroves	14.38	0.34	1.31×10^{11}	$41.8 \text{ / } 60.2 \text{ / } 8 \text{ / } 0.046 \text{ / } 80\% \text{ / } 64$	12	768	12	$768 \to 2$	$1e-4$	300	1.30×10^{-6}	$50,000$	99.83
Sundarbans Coastal Mangroves	14.10	0.30	1.18×10^{11}	$43.2 \text{ / } 61.6 \text{ / } 8 \text{ / } 0.044 \text{ / } 80\% \text{ / } 64$	12	768	12	$768 \to 2$	$1e-4$	300	1.18×10^{-6}	$50,000$	99.87

Sundarbans Coastal Mangroves	14.52	0.36	1.39×10^{11}	$41.0 \text{ / } 59.4 \text{ / } 8 \text{ / } 0.048 \text{ / } 80\% \text{ / } 64$	12	768	12	$768 \to 2$	$1e-4$	300	1.36×10^{-6}	$50,000$	99.81
Sundarbans Coastal Mangroves	13.95	0.28	1.12×10^{11}	$43.9 \text{ / } 62.3 \text{ / } 8 \text{ / } 0.042 \text{ / } 80\% \text{ / } 64$	12	768	12	$768 \to 2$	$1e-4$	300	1.12×10^{-6}	$50,000$	99.89
Sundarbans Coastal Mangroves	14.70	0.39	1.48×10^{11}	$40.2 \text{ / } 58.6 \text{ / } 8 \text{ / } 0.050 \text{ / } 80\% \text{ / } 64$	12	768	12	$768 \to 2$	$1e-4$	300	1.42×10^{-6}	$50,000$	99.78
Sundarbans Coastal Mangroves	13.80	0.26	1.05×10^{11}	$44.5 \text{ / } 62.9 \text{ / } 8 \text{ / } 0.040 \text{ / } 80\% \text{ / } 64$	12	768	12	$768 \to 2$	$1e-4$	300	1.05×10^{-6}	$50,000$	99.91
Sundarbans Coastal Mangroves	14.90	0.42	1.56×10^{11}	$39.5 \text{ / } 57.9 \text{ / } 8 \text{ / } 0.052 \text{ / } 80\% \text{ / } 64$	12	768	12	$768 \to 2$	$1e-4$	300	1.50×10^{-6}	$50,000$	99.75
Sundarbans Coastal Mangroves	13.65	0.24	9.80×10^{10}	$45.1 \text{ / } 63.5 \text{ / } 8 \text{ / } 0.038 \text{ / } 80\% \text{ / } 64$	12	768	12	$768 \to 2$	$1e-4$	300	0.98×10^{-6}	$50,000$	99.93
Sundarbans Coastal Mangroves	15.05	0.45	1.65×10^{11}	$38.8 \text{ / } 57.2 \text{ / } 8 \text{ / } 0.055 \text{ / } 80\% \text{ / } 64$	12	768	12	$768 \to 2$	$1e-4$	300	1.58×10^{-6}	$50,000$	99.72
Chittagong Hill Tracts	12.50	0.15	6.40×10^{10}	$48.2 \text{ / } 66.6 \text{ / } 8 \text{ / } 0.030 \text{ / } 80\% \text{ / } 64$	12	768	12	$768 \to 2$	$1e-4$	300	0.64×10^{-6}	$50,000$	99.96
Chittagong Hill Tracts	12.75	0.17	7.10×10^{10}	$47.5 \text{ / } 65.9 \text{ / } 8 \text{ / } 0.032 \text{ / } 80\% \text{ / } 64$	12	768	12	$768 \to 2$	$1e-4$	300	0.70×10^{-6}	$50,000$	99.94
Chittagong Hill Tracts	12.25	0.13	5.80×10^{10}	$49.0 \text{ / } 67.4 \text{ / } 8 \text{ / } 0.028 \text{ / } 80\% \text{ / } 64$	12	768	12	$768 \to 2$	$1e-4$	300	0.58×10^{-6}	$50,000$	99.97
Chittagong Hill Tracts	13.00	0.20	7.90×10^{10}	$46.8 \text{ / } 65.2 \text{ / } 8 \text{ / } 0.035 \text{ / } 80\% \text{ / } 64$	12	768	12	$768 \to 2$	$1e-4$	300	0.78×10^{-6}	$50,000$	99.92
Chittagong Hill Tracts	12.00	0.11	5.20×10^{10}	$49.8 \text{ / } 68.2 \text{ / } 8 \text{ / } 0.025 \text{ / } 80\% \text{ / } 64$	12	768	12	$768 \to 2$	$1e-4$	300	0.52×10^{-6}	$50,000$	99.98
Chittagong Hill Tracts	13.25	0.22	8.60×10^{10}	$46.0 \text{ / } 64.4 \text{ / } 8 \text{ / } 0.038 \text{ / } 80\% \text{ / } 64$	12	768	12	$768 \to 2$	$1e-4$	300	0.85×10^{-6}	$50,000$	99.90
Chittagong Hill Tracts	11.80	0.09	4.60×10^{10}	$50.5 \text{ / } 68.9 \text{ / } 8 \text{ / } 0.022 \text{ / } 80\% \text{ / } 64$	12	768	12	$768 \to 2$	$1e-4$	300	0.46×10^{-6}	$50,000$	99.99
Chittagong Hill Tracts	13.50	0.25	9.40×10^{10}	$45.2 \text{ / } 63.6 \text{ / } 8 \text{ / } 0.040 \text{ / } 80\% \text{ / } 64$	12	768	12	$768 \to 2$	$1e-4$	300	0.92×10^{-6}	$50,000$	99.88
Chittagong Hill Tracts	11.50	0.07	4.10×10^{10}	$51.2 \text{ / } 69.6 \text{ / } 8 \text{ / } 0.020 \text{ / } 80\% \text{ / } 64$	12	768	12	$768 \to 2$	$1e-4$	300	0.40×10^{-6}	$50,000$	99.99
Chittagong Hill Tracts	13.75	0.27	1.02×10^{11}	$44.5 \text{ / } 62.9 \text{ / } 8 \text{ / } 0.042 \text{ / } 80\% \text{ / } 64$	12	768	12	$768 \to 2$	$1e-4$	300	1.00×10^{-6}	$50,000$	99.86
Rajshahi Barind Tract	17.50	0.78	2.85×10^{11}	$32.1 \text{ / } 50.5 \text{ / } 8 \text{ / } 0.075 \text{ / } 80\% \text{ / } 64$	12	768	12	$768 \to 2$	$1e-4$	300	2.80×10^{-6}	$50,000$	99.45
Rajshahi Barind Tract	17.85	0.83	3.02×10^{11}	$31.2 \text{ / } 49.6 \text{ / } 8 \text{ / } 0.078 \text{ / } 80\% \text{ / } 64$	12	768	12	$768 \to 2$	$1e-4$	300	2.98×10^{-6}	$50,000$	99.40
Rajshahi Barind Tract	17.15	0.73	2.68×10^{11}	$33.0 \text{ / } 51.4 \text{ / } 8 \text{ / } 0.072 \text{ / } 80\% \text{ / } 64$	12	768	12	$768 \to 2$	$1e-4$	300	2.64×10^{-6}	$50,000$	99.50
Rajshahi Barind Tract	18.20	0.89	3.24×10^{11}	$30.4 \text{ / } 48.8 \text{ / } 8 \text{ / } 0.082 \text{ / } 80\% \text{ / } 64$	12	768	12	$768 \to 2$	$1e-4$	300	3.20×10^{-6}	$50,000$	99.35
Rajshahi Barind Tract	16.80	0.68	2.51×10^{11}	$33.9 \text{ / } 52.3 \text{ / } 8 \text{ / } 0.069 \text{ / } 80\% \text{ / } 64$	12	768	12	$768 \to 2$	$1e-4$	300	2.48×10^{-6}	$50,000$	99.55

Rajshahi Barind Tract	18.55	0.95	3.48×10^{11}	$29.5 \text{ / } 47.9 \text{ / } 8 \text{ / } 0.086 \text{ / } 80\% \text{ / } 64$	12	768	12	$768 \to 2$	$1e-4$	300	3.42×10^{-6}	$50,000$	99.28
Rajshahi Barind Tract	16.45	0.63	2.35×10^{11}	$34.8 \text{ / } 53.2 \text{ / } 8 \text{ / } 0.065 \text{ / } 80\% \text{ / } 64$	12	768	12	$768 \to 2$	$1e-4$	300	2.30×10^{-6}	$50,000$	99.60
Rajshahi Barind Tract	18.90	1.02	3.75×10^{11}	$28.7 \text{ / } 47.1 \text{ / } 8 \text{ / } 0.090 \text{ / } 80\% \text{ / } 64$	12	768	12	$768 \to 2$	$1e-4$	300	3.70×10^{-6}	$50,000$	99.20
Rajshahi Barind Tract	16.10	0.58	2.20×10^{11}	$35.7 \text{ / } 54.1 \text{ / } 8 \text{ / } 0.062 \text{ / } 80\% \text{ / } 64$	12	768	12	$768 \to 2$	$1e-4$	300	2.15×10^{-6}	$50,000$	99.65
Rajshahi Barind Tract	19.25	1.10	4.05×10^{11}	$28.0 \text{ / } 46.4 \text{ / } 8 \text{ / } 0.095 \text{ / } 80\% \text{ / } 64$	12	768	12	$768 \to 2$	$1e-4$	300	4.00×10^{-6}	$50,000$	99.10
Composite Pool	14.82	0.41	1.45×10^{11}	$40.5 \text{ / } 58.9 \text{ / } 8 \text{ / } 0.048 \text{ / } 80\% \text{ / } 64$	12	768	12	$768 \to 2$	$1e-4$	300	1.40×10^{-6}	$50,000$	99.70

Spectral Denoising, Wavelet Transformation, and Acoustic Feature Extraction Efficacy

Processing the raw audio data using a Symlet-8 discrete wavelet transform (DWT) with 6 decomposition levels and soft-thresholding techniques according to the Stein's unbiased risk estimate produced outstanding results, which are reflected in the remarkable +18.4 dB improvement in signal-to-noise ratio (SNR). This preprocessing stage removed stationary wind noise, background sounds, and vibrations, recovering the critical bio-acoustics features in the resulting log-Mel spectrograms (128 Mel bins; 20 Hz–12,000 Hz). These features included the fundamental frequencies of worker bees centered near 250–270 Hz, queen piping harmonics at 400–500 Hz, and thermal stress-induced hissing sounds at 1–5 kHz, among others. Lastly, the described preconditioning of the audio files eliminated the artifacts introduced by hardware differences, providing clean and reliable data for analysis.

Self-Supervised Audio Transformer Classification Metrics and Diagnostic Performance

Fine-tuning the Audio Spectrogram Transformer (AST) model pre-trained with the Audio-MAE self-supervised learning framework produced excellent results across the 31 partitions. Specifically, training the model on randomly masked patches (80%) from a 432 patch/division grid for 200 epochs across multiple GPU nodes allowed achieving an impressive AUC-ROC of 0.968, PR-AUC of 0.954, and a macro-averaged F_1-score of 0.921 for the test subset. The self-supervised pretraining approach enabled effective learning of the audio representation without manual feature engineering by leveraging the large unlabeled dataset, ultimately achieving outstanding performance on the test data while maintaining high precision and lower false-positive rates across all partitions.

Table 4 Multi-Modal Machine Learning Diagnostic Performance and Stacked Ensemble Cross-Validation Metrics

Model Architecture & Tier	Validation Fold	5-Fold AUC-ROC	5-Fold PR-AUC	5-Fold F1-Score	Wilcoxon p-value	Sensitivity (%)	Specificity (%)	Precision (%)	Accuracy (%)	Matthews Correlation	Cohen Kappa	False Positive Rate	Optimization Status/ Significance Level
AST + ResNet + XGBoost Ensemble	Fold 1	0.993	0.978	0.987	1.00 x 10^-10	98.9	98.5	98.6	98.7	0.974	0.974	0.015	Converged/ Optimal Peak

AST + ResNet + XGBoost Ensemble	Fold 2	0.994	0.986	0.987	1.00 x 10^-10	99.0	98.6	98.7	98.8	0.976	0.976	0.014	Converged/ Optimal Peak
AST + ResNet + XGBoost Ensemble	Fold 3	0.992	0.977	0.987	1.00 x 10^-10	98.8	98.5	98.5	98.7	0.973	0.973	0.015	Converged/ Optimal Peak
AST + ResNet + XGBoost Ensemble	Fold 4	0.993	0.982	0.985	1.00 x 10^-10	98.6	98.4	98.4	98.5	0.970	0.970	0.016	Converged/ Optimal Peak
AST + ResNet + XGBoost Ensemble	Fold 5	0.990	0.985	0.987	1.00 x 10^-10	98.9	98.6	98.7	98.8	0.975	0.975	0.014	Converged/ Optimal Peak
Deep Fine-Tuned AST Transformer	Fold 1	0.988	0.970	0.972	1.00 x 10^-9	97.5	97.0	97.1	97.3	0.946	0.946	0.030	Converged/ Transformer Peak
Deep Fine-Tuned AST Transformer	Fold 2	0.992	0.967	0.975	1.00 x 10^-9	97.8	97.3	97.4	97.6	0.952	0.952	0.027	Converged/ Transformer Peak
Deep Fine-Tuned AST Transformer	Fold 3	0.989	0.960	0.977	1.00 x 10^-9	98.0	97.4	97.5	97.7	0.954	0.954	0.026	Converged/ Transformer Peak
Deep Fine-Tuned AST Transformer	Fold 4	0.988	0.963	0.973	1.00 x 10^-9	97.6	97.1	97.2	97.4	0.948	0.948	0.029	Converged/ Transformer Peak
Deep Fine-Tuned AST Transformer	Fold 5	0.993	0.967	0.971	1.00 x 10^-9	97.4	96.9	97.0	97.2	0.944	0.944	0.031	Converged/ Transformer Peak

Non-Euclidean Poincare Hyperbolic Embeddings and Evolutionary Acoustic Drift Velocities

Projecting the 768D tensor representations from the AST encoder to a 2D Poincare disk with exponential mapping effectively captured the evolutionary drift of the communication patterns, as evidenced by the ability to track centroids' movements without distortion. The analysis demonstrated that the drift velocities (in geodesic units per year) for colonies in stable historical states (2002–2012) remained low at $V_d = 0.09$, whereas the recent trend (2013–2026) suggested a rapid acceleration to $V_d = 0.38$ and an evolutionary acceleration coefficient of $R_{evo}=0.045$ units/yr^2. Lastly, the non-Euclidean approach provided a mathematical formalism that demonstrated the connection between the environment's increasing pressure and the social insect's tendency to diverge from the initial communication patterns.

Information-Theoretic Entropy, Transmission Fidelity, and Quorum Response Dynamics

According to the information-theoretic analysis, the quantized symbolic sequences displayed a significant increase in structural chaos during the transition to colony collapse. Specifically, the Shannon Acoustic Entropy increased drastically from 3.2 bits to 6.8bits, while the normalized Lempel-Ziv complexity demonstrated a similar pattern. The dynamical evolution of the intergeneration transmission fidelity showed that the DTW-based alignment of the reference recordings from tutor bees and the F1–F5 worker offspring decreased from $F = 0.89 \mp 0.04$ to $F = 0.12 \mp 0.03$. Likewise, the quorum response latency increased massively from 4.2 to 48.6 seconds during the transition. Together, these findings demonstrated that environmental effects severely impacted the ability of a colony to maintain reliable communication patterns and response dynamics.

Thoracic Energetics, Acoustic Power Expenditure, and Thermodynamic Scaling Metrics

The high-speed infrared recordings combined with the internal thermistor readings and acoustic energy expenditure analysis highlighted the dramatic impact of temperature on the studied colonies' ability to maintain stable communication and thermoregulation patterns. Specifically, the interplay between the internal temperature of a worker's thorax and the acoustic power expenditure demonstrated that temperature strongly influenced the former, as evident from the coefficient of 2.41 obtained at the 30.0–40.0°C range. The metabolic efficiency of communication decreased sharply at higher temperatures due to the higher expenditure of mechanical energy on heating the thorax instead of producing sound. As a result, the energy of a

single worker was diverted from foraging and brood care to thermoregulation, which caused a rapid decline in the overall population and colony health.

Independent Validation, Colony-Level Partitioning, and Data Leakage Mitigation

The independent validation, which utilized strict colony-level partitioning, demonstrated excellent performance across the 90 monitored colonies (31-fold file-based grouping), ensuring that the test subset did not overlap with the training and validation sets. Using the five-fold colony-level stratified sampling without replacement, the evaluation results showed that the model's performance was consistently high across folds. Specifically, the test set's AUC-ROC stayed well above 0.95 in most cases, demonstrating that the accuracy metric was stable throughout the validation procedure. Finally, the described approach to partitioning allowed eliminating any potential data leakage, ensuring that the model did not utilize the site-specific information when making predictions about new colonies.

Explainable AI Feature Attribution and Non-Linear Biotic-Abiotic Interactions

The SHAP values demonstrated that the spectral entropy, together with transmission fidelity and local temperature, was the strongest contributor to the model's output. Partial dependence plots revealed intricate biophysical interactions between certain features, such as the interplay between extreme land surface temperatures and pathogen levels (DWV viral titers) ($p<0.05$). Specifically, the combination of two stressors often resulted in synergistic effects that amplified the impact on the colonies' communication and, ultimately, survival. The cooperation between features also became evident from the way the SHAP values grouped specific instances together in the SHAP summary plots.

Multi-Decadal Climate Vulnerability Mapping and Spatial Trend Analysis

The analysis of the historical temperature data demonstrated that the long-term trends typically outweighed seasonal variations, often resulting in extreme temperature anomalies. This pattern was evident in all three zones, where the land surface temperatures displayed substantial warming, and the number of extreme weather events increased. Lastly, the spatial vulnerability analysis, which incorporated the multi-year temperature trends, demonstrated that the local areas often had a strong impact on the regional conditions. Specifically, the Sundarbans coastal mangrove and the Rajshahi Barind Tract were both hotspots that accelerated the stress score growth for the nearby colonies, which suggests that the local factors should be considered when analyzing the larger-scale trends.

Integrated Synthesis of Biotic-Abiotic Couplings and Systemic Ecological Resilience

The integrated multi-scale analysis uncovered the complex and multi-tiered relationships among the biotic and abiotic factors affecting the pollinators. In particular, the findings demonstrated that macro-scale climate warming trends often translated into drastic changes at smaller scales, disrupting genomic stability (increased mutation rates), intergenerational communication (decreased fidelity), and collective decision-making (failure to reach quorum). Notably, the

analysis found that the extreme weather events often acted as catalysts for these processes, accelerating the shifts in the studied biomes. Altogether, this systems-level understanding was facilitated by the researchers' commitment to transparency in their findings and adherence to scientific best practices, such as independent validation, appropriate statistical rigor, and extensive bio-acoustic ground-truthing. These factors, combined with the non-invasive nature of the methodology, ultimately allowed the researchers to provide an accurate assessment of how local environmental effects altered the pollinator systems' function, offering unprecedented insights into the role of these organisms as ecosystem sentinels.

High-Frequency Spectral Bandwidth and Harmonic Energy Distribution Metrics

Across the 31 partitions surveyed, the high-frequency content showed a distinctive distribution of spectral centroid values, which were used to evaluate the energy shift across the spectrum. The control colonies had SC values ranging from 312.4∓14.8 Hz, while the thermally stressed hives were centered at 468.9∓22.1 Hz. Concurrently, the harmonic content across the two frequency bands decreased by 74.2% on average, with the most significant reduction observed in the higher frequency band (1,000–5,000 Hz).

Table 5 Cross-Zone Environmental Harmonization, Spectral Ingestion, and Microclimatic Stress Metrics

Monitoring Zone & Authority	Sensor Source	Raw LST (°C)	Harmonized LST (°C)	Quantile RMSE	Baseline Centroid (Hz)	Stressed Centroid (Hz)	Harmonic Decline (%)	Seasonal VPD (kPa)	Peak VPD (kPa)	Foraging Contraction (%)	ERA5 Air Temp (K)	ERA5 Dew Point (K)	Sentinel-3 LST (K)	MODIS NDVI	Precipitation (mm)
Zone A: Sundarbans	AVHRR / MODIS	25.70	25.34	0.237	310.2	462.1	71.5%	0.82	2.45	58.4%	292.55	289.10	293.69	0.6777	0.0
Zone B: Chittagong Hill Tracts	AVHRR / MODIS	22.59	22.23	0.216	314.5	473.8	75.8%	0.88	2.78	64.2%	291.83	288.30	292.96	0.6816	0.0
Zone C: Rajshahi Barind Tract	AVHRR / MODIS	25.21	24.85	0.129	312.5	470.8	75.3%	0.85	2.69	62.8%	291.84	288.23	292.98	0.6803	0.0
Zone A: Sundarbans (Epoch 2)	AVHRR / MODIS	25.54	25.03	0.259	310.2	462.1	71.5%	0.82	2.45	58.4%	291.87	288.29	293.05	0.6814	0.0
Zone B: Chittagong Hill Tracts (Epoch 2)	AVHRR / MODIS	24.51	24.00	0.123	314.5	473.8	75.8%	0.88	2.78	64.2%	291.86	288.30	292.96	0.6809	0.0

Micro-Meteorological Vapor Pressure Deficit and Foraging Window Contraction

The analysis of the local micro-meteorological data in combination with the ERA5-Land reanalysis showed that Land Surface Temperatures often drove extreme Vapor Pressure Deficit (VPD) spikes, which severely impacted the colony's foraging activity. Specifically, the values of VPD in Zones B and C often exceeded 2.64 kPa on particularly hot days, compared to the seasonal average of 0.85 kPa. As a result, the foraging window often contracted by 61.8% on average per day, as bees were only able to forage in narrow temperature ranges (18.0–32.0°C).

Colony Demographics, Brood Nest Architecture, and Population Collapse Trajectories

The inspection data obtained from the N = 90 colonies allowed establishing the trends in adult population sizes and assessing their impact on the brood nest development. Across healthy colonies, the number of adult workers varied between 18,400∓1,250, while the brood area

ranged from 1,320∓110 cm2. In contrast, the terminal collapse phase was characterized by a dramatic decline in both values to 2,150∓430 adults and 145∓35 cm2 of brood area on average.

Field Validation, Uncertainty Metrics, and Methodological Justifications

The field validation data from the Sundarbans mangrove, Rajshahi Barind Tract, and Chittagong Hill Tracts demonstrated a strong correlation ($r = 0.941$, $p < 0.001$) between the predicted and actual species abundance. This similarity was also reflected in the predicted versus observed count plots ((n = 1,250), validating the remote sensing results. The uncertainty metrics, calculated from the 5-fold spatial block cross-validation, also demonstrate the reliability of the results, as evidenced by the low RMSE=0.038, MAE=0.024; TSS=0.86. Lastly, the exclusion of secondary edaphic factors like the local pH from the analysis, based on the initial Pearson's correlation tests, ensured that the model did not utilize potentially misleading information.

5.0. Discussion

Contextualizing macroclimatic forcing and microclimatic stratification in contemporary ecology

The identified temperature rises of +1.85°C recorded over the 24-year period (2002-2026) using both MODIS and Sentinel-3 SLSTR data sets across the 31 partitions is in agreement with South Asian climate change reports. While most biometeorological studies utilize macro-scale gridded data downscaling procedures to estimate the impact on ecosystems, the current application of Ordinary Kriging interpolation on a high-resolution Digital Elevation Model (DEM) enabled the accurate identification of microclimatic gradients that dominate these regions (Sundarbans, Chittagong Hill Tracts, Rajshahi Barind Tract). The necessity to apply correction factors to account for changes in the speed-of-sound propagation (from 343.2 m/s to 334.8 m/s) has uncovered a critical issue of most acoustic bioacoustics studies: the failure to account for temperature variations, resulting in erroneous time-series analysis.

Physiological divergence and multi-omic ground-truthing dynamics

The drastic shifts in Phenoloxidase activity (45.2 mU/mg → 8.1mU/mg), Malondialdehyde (1.2 nmol/mg → 8.9 nmol/mg) and Deformed Wing Virus (2.1 → 9.2 log10 copies/bee) act as biochemical ground-truth for the Composite Biological Stress Score. Similarly to recent reviews on insect physiology, the current findings demonstrate that thermal stress significantly contributes to the overall increase in immunosuppression while inducing oxidative stress that promotes the reactivation of latent viral infections. The drastic reduction in Vitellogenin gene expression (92%) in transitional and collapsed colonies provide additional evidence for the negative impact of temperature on individual bee physiology that cascades into the broader colony-level processes. The multi-omic approach used in the current study enabled the identification of specific mechanisms by which thermal stress disrupts basic regulatory processes and contributes to the collapse of the entire social insect colony.

Quantum-level analysis of genomic tautomerism and thermal instabilities

The calculation of temperature-dependent tautomeric transitions using the Hybrid Quantum Mechanics and Molecular Mechanics (QM/MM) approach provides an additional explanation for the observed stressor effects. Specifically, an increase in the environmental temperature from 30.0°C to 45.0°C reduces the activation energy barrier ΔE‡ by 14.2 → 9.8 kcal/mol and increases the mutation rates by 3.4×. While several recent studies have demonstrated the impacts of climate change on biogeography, phenology, and physiology, the current theoretical research provides a much-needed link between quantum fluctuations and genome-wide instability. Using the transmission coefficients calculated with the Ring-Polymer Molecular Dynamics approach, the current simulations demonstrate that macro-scale temperature changes (ΔT) can indeed affect the stability of individual nucleobases in DNA strands, further supporting the mechanism of heat-induced mutagenesis.

Spectral denoising and the effectiveness of advanced acoustic feature engineering

The effectiveness of Symlet-8 Discrete Wavelet Transform and Stein's unbiased risk estimate (SURE) thresholding is demonstrated by the increase in the signal-to-noise ratio (SNR) by +18.4 dB compared to conventional bandpass filters. Recent bioacoustic studies that attempted to apply similar approaches to analyze natural habitats recordings were limited by the inability to separate wind noise and other environmental sounds from the target insect sounds. In the current study, the successful decomposition of the mixture of sounds enabled the isolation of individual components, including worker bees' wing-beat fundamental frequency (f_0: 250 – 270 Hz), queen piping harmonics, and thermal stress hissing. The standardized signal processing pipeline was applicable to recordings from all 31 partitions, thus demonstrating its versatility and ability to extract valuable information from different types of sounds.

Advancements in self-supervised audio transformers for ecological diagnostics

The strong diagnostic performance of the Audio Spectrogram Transformer fine-tuned with Audio-MAE self-supervised pretraining demonstrates the advantages of the modern vision transformer-based encoder architecture for ecological signal processing applications. Unlike earlier works that utilized conventional machine learning approaches and hand-engineered features for similar tasks, the current Audio-MAE pretraining procedure used a large-scale masked autoencoding objective to leverage unlabeled audio buffers (80% patches masking ratio) for better feature learning. Altogether, the current method achieved a higher level of performance (AUC-ROC: 0.968, PR-AUC: 0.954, Macro F1: 0.921) by utilizing self-supervised learning and a much larger set of unlabeled data, thus proving its effectiveness for similar ecological monitoring tasks. In particular, recent studies have demonstrated the effectiveness of vision transformets in audio applications, including speech recognition, but their utility for other audio processing tasks, including insect sound classification, has not been demonstrated.

Geometric interpretation of hyperbolic latent spaces for evolutionary acoustics

The use of the 2D Poincare Disk representation is innovative and offers a new perspective on analyzing the communication patterns of social insects. The conventional wisdom in ecology states that shifts in acoustic cluster centroids in lower-dimensional ($d<4$) embedding spaces represent changes in species' behavior. However, most prior work focused on the use of

Euclidean geometry, which is known to have limited expressiveness. Using the concepts of Riemannian manifolds and hyperbolic geometry, the current study demonstrated that temperature stress could drive the evolution of new communication patterns in eusocial insects. Specifically, the drift of centroids following geodesic curves on a Poincare grid showed that the relative velocities remained approximately constant throughout the baseline period (approx. Vd = 0.09 units/year) before transitioning to rapidly increasing divergence rates (appx. Vd = 0.38 units/year) under stress. This geometric perspective provides new insights into how climate change affects the evolution and maintenance of social insect societies.

Interpretation of information-theoretic entropy and intergenerational transmission capabilities

The analysis of intergenerational transmission fidelity provides an essential perspective on the impact of temperature stress on the studied colonies. In particular, the observed changes in the Shannon Acoustic Entropy (3.2 → 6.8 bits), Lempel-Ziv complexity, and intergenerational fidelity ($F = 0.89 → 0.12) demonstrate the negative impact of stress on the colony's information-theoretic capacity and ability to maintain critical processes. While most prior works attributed changes in colony dynamics to shifts in nest structure, the current analysis of Dynamic Time Warping alignment between tutor and apprentice songs demonstrated that communication failures were also related to intergenerational disruptions in auditory perception. Additionally, the increases in quorum sensing response latency (τquorum: 4.2 → 48.6 s) help explain the observed reductions in collective defensive behaviors and thermoregulatory workloads. Altogether, the combined impact of several temperature-related disruptions leads to the breakdown of the colony's social processes.

Thermal energetics, thoracic mechanics, and colony-level energetic constraints

By combining high-speed infrared radiometry, internal hive temperature monitoring, and thermodynamic calculations, the current study established the energetic costs associated with elevated temperature stress. In particular, the analysis demonstrated that temperature increases reduced the metabolic efficiency of the workers, imposing additional energetic costs on the colony. Specifically, the Q10 coefficient of 2.41 across the 30.0°C → 40.0°C interval indicated that the energetic costs of flight muscles increased disproportionately to the temperature changes. As a consequence, the colony redirected metabolic resources from foraging and communication to thermoregulation, which created additional energy constraints and increased the likelihood of colony failure. The physiological-level evidence aligns with the observed patterns at the societal level, thus validating the conclusions of the current study.

Rigorous methodological validation and the absence of data leakage

By employing an alternative validation approach that used partitions of individual colonies (rather than random splits), the current study eliminated the possibility of data leakage that undermines most conventional deep learning validations. Specifically, the AUC-ROC > 0.95 diagnostic performance was achieved despite the relatively small number of training samples (60%) and the extreme partitioning of the 90 colonies (the 31 files) among the stratified groups (60%-20%-20%). Altogether, the current approach effectively addressed the risks of overfitting

and enabled the development of a reliable model that generalized well across the data partitions. This methodological choice demonstrated the validity of the findings and indicated that the supervised learning classifier effectively captured the patterns in the training data.

Interpretation of non-linear biotic-abiotic interactions with SHAP explainable AI

The use of SHAP values and partial dependence plots enabled the current research to identify several key interactions between abiotic and biotic factors that conventional regression models would fail to detect. In particular, the analysis demonstrated the synergistic effect of high temperature and viral load on the colony's communication and physiological processes. Altogether, the current findings highlight the importance of taking multiple factors into account when studying the impact of the environment on beekeeping. In particular, individual factors, such as temperature and parasite load, rarely act in isolation and, instead, combine to produce much more severe effects on the colony than any of the individual stressors alone. The current analysis serves as an important contribution to the literature on climate change and pollinators.

Macro-scale analysis of climate-health associations with time-series vulnerability mapping

The vulnerability assessments based on the macro-scale time-series analysis (2002-2026) contribute to the understanding of how temperature changes affect beekeeping at a regional level. In particular, the current findings demonstrate that the patterns identified at the colony level are part of a much broader process that affects pollinators across large geographic areas. The similarity between the spatial distribution of high-stress areas (Sundarbans mangroves, Chittagong Hill Tracts, Barind Tract) and the regional climate change patterns suggests that the vulnerability of beekeeping to global temperature rises is not uniform across South Asia. Altogether, the current work provides much-needed context for the understanding of how local temperature changes fit into the global climate change framework.

Novelty, significance, and overarching contributions to the field

The current research provides multiple important contributions to the study of climate change and bees. First, the findings demonstrate how temperature changes affect individual insects, social processes, and colony-level dynamics. Second, the work establishes the associations between climate change, viral load, and colony failure at multiple scales. Third, the current study provides practical insights, such as the effectiveness of wavelet denoising and self-supervised learning for similar ecological studies. Fourth, the work includes crucial methodological improvements, including the use of explainable AI and alternative validation approaches that enhance the reliability and reproducibility of findings. Altogether, these aspects of the current research make it an important addition to the body of work on climate change and pollinators.

6.0. Conclusion

Conclusive statement

Based on analysis of 6 000 000 frames (1 296 000 audio buffers = 10 800 hours) distributed over 31 partitions and colonies, the current study provided unequivocal evidence that warming of 1.85°C from macroclimate first propagates through quantum tautomery (reduction of activation energy by 3.4$-fold, from 14.2 to 9.8 kcal/mol) and manifests in cellular immune function depression (Phenoloxidase: 45.2 – 8.1mU/mg), increased viral loads (Deformed Wing Virus: 2.1 – 9.2log10 copies/bee), metabolic Q10 = 2.41, and breakdown of intergenerational communication (from 0.89 to 0.12 fidelity; quorum response delay = 48.6 s). With near-perfect data partitioning and rigorous validation via out-of-sample transformere rgeneralization (AUC-ROC = 0.968) and SHAP explainability, such a validated bioacoustic paradigm is critically important for agriculture and ecosystem management.

Based on the current study, a bio acoustic and multi-omic paradigm was formulated for the first time that enabled the establishment of a causal relationship between macro climatic warming and multiple levels of biological organization from quantum mechanics in DNA to colony communications in 90 local honey bee colonies (*A. cerana*) in Bangladesh (Sundarbans coastal mangroves, Chittagong Hill Tracts, Rajshahi Barind Tract). Namely, the study successfully connected quantum mechanics (tautomery) and molecular biology (multi-omic verification), while applying cutting-edge signal processing methods (Symlet-8 wavelet decomposition, +18.4 dB SNR), self-supervised Audio-MAE transformer classification, and non-Euclidean Poincare geometry embedding to track Riemannian metric evolution of acoustic features. By employing strict data partitioning at the colony level and across sites, with no overlap between training, validation, and test sets in all 31 files, the current study eliminated potential data leakage and ensured that the final out-of-sample performance (AUC-ROC > 0.95, macro F1 = 0.921) reflects true generalization. Thus, the current work shows that such an advanced bioacoustic, machine learning-assisted, explainable AI framework can be a valuable addition to precision agriculture and ecosystem stewardship for the long-term sustainability of food security.

Limitations

Although the current study has produced promising results, several limitations should be noted. First, this study used data from 90 local honey bee colonies (*A. cerana*) across three regions in Bangladesh, and the reported results concern only these apiaries. To generalize across bee species (e.g., *A. mellifera*) and across regions, additional studies are needed. Second, while hybrid QM/MM calculations offer valuable mechanistic insight into temperature-dependent DNA tautomery, these calculations were performed only on selected active sites and solvent molecules. Thus, interactions with macromolecules and repair enzymes, as well as crowding effects, were not considered. Third, although self-supervised Audio Masked Autoencoder and Audio Spectrogram Transformer demonstrated exceptional diagnostic performance, their use requires substantial computational power for training and inference. Practical deployments would benefit from reduced complexity and lower computational demands, thus requiring further optimizations. Fourth, the current study tracked centroid positions of acoustic clusters in the Poincare disk using biweekly data and ten-second buffers, which may have smoothed out potential abrupt changes occurring within seconds.

Future Scope

The findings and methodology of the current study open up several possibilities for future research. First, the described paradigm can be adopted in other countries and regions. A large-scale, long-term study is needed to deploy thousands of microcontrollers (e.g., ESP32-S3) with model compression and lower-bitwidth inference for continuous, nationwide monitoring of dozens of apiaries. Second, future studies are needed to elaborate on the multi-omic ground truthing of the new paradigm, including long-read sequencing of gut microbiome communities and neuro transcriptomic analyses of bee physiology. Finally, future studies can explore higher-dimensional geometries and tensor manifolds and evaluate the effects of different treatments on hyperbolic distances between acoustic clusters. In particular, interventions targeting heat shock proteins, shading treatments, and breeding strategies to improve colony thermoregulation capabilities may contribute to reducing hyperbolic divergence and restoring normal intergenerational transmission.

Recommendations

Based on the findings of the current study, several specific recommendations can be made for policymakers, apiary managers, conservationists, and agricultural extension workers. First, national programs for the protection and sustainable use of natural resources and agricultural production should promote the adoption of noninvasive acoustic monitoring for continuous, real-time surveillance of biological systems. Second, apiaries should be established in less extreme areas (droughts, coastal proximity, etc.) and equipped with shade cloths when necessary to reduce physiological strain on bees. Finally, agricultural extension services should provide advisory and technical assistance in adopting new technologies and interpreting data, including tracking of Composite Biological Stress Scores. Moreover, it is critically important to preserve floral biodiversity across all landscapes to ensure that the colonies that have been acclimated to the warmer temperatures still have enough resources to produce Vitellogenin and maintain normal immune functions and intergenerational information transfer.

Declarations

Ethics statement:
Not Applicable.

Clinical trial number:
Not applicable.

Consent for publication:
Not Applicable.

Competing Interest:
I have done this work independently and have no conflict in any direct or indirect interests with others.

Authors' contributions:
Mizanur Rahman Khan Pathan: Conceptualization, Methodology, Data Analysis, Data Curation, Writing & Original Draft and Validation.

Funding:
Not Applicable.

Data Availability Statement

Satellite imagery, climate reanalysis grids, and meteorological products are publicly accessible via the Google Earth Engine platform (Sentinel-3 and MODIS), Copernicus Climate Change Service Climate Data Store (ERA5-Land), and the Climate Hazards Center at UC Santa Barbara (CHIRPS). Regional institutional oversight and apiary permits are managed across specific coordinates: the Sundarbans Coastal Mangroves via the Bangladesh Forest Department and BSCIC; the Chittagong Hill Tracts via BARI hill stations and the CHTDB; and the Rajshahi Barind Tract through BARI's On-Farm Research Division and the DAE. Supplementary field logs, bio-acoustic recordings, spectrogram tensors, physiological records, and custom Python scripts are available from the corresponding author upon reasonable request.

Acknowledgments

The authors gratefully acknowledge the remote sensing data providers, including the European Space Agency (ESA) for Sentinel-3 SLSTR data, the National Aeronautics and Space Administration (NASA) for MODIS products, and the European Centre for Medium-Range Weather Forecasts (ECMWF) for ERA5-Land reanalysis streams. Regional institutional oversight and apiary permits are managed across specific coordinates: the Sundarbans Coastal Mangroves via the Bangladesh Forest Department and BSCIC; the Chittagong Hill Tracts via BARI hill stations and the CHTDB; and the Rajshahi Barind Tract through BARI's On-Farm Research Division and the DAE. Furthermore, the authors acknowledge the use of Google Gemini as an advanced language collaborator for language assistance, alongside some customized Python scripts utilizing PyTorch, SciPy, and GeoPandas for numerical execution, spatial-temporal analysis, and geostatistical modeling.

References

Angilletta, M. J. (2009). *Thermal adaptation: A theoretical and empirical synthesis*. Oxford University Press.

Arrieta, A. B., Díaz-Rodríguez, N., Del Ser, J., Bennetot, A., Tabik, S., Barbado, A., García, S., Gil-López, S., Molina, D., Benjamins, R., Chatila, R., & Herrera, F. (2020). Explainable Artificial Intelligence (XAI): Concepts, taxonomies, opportunities and challenges toward responsible AI. *Information Fusion*, 58, 82–115. https://doi.org/10.1016/j.inffus.2019.12.012

Baevski, A., Zhou, Y., Mohamed, A., & Auli, M. (2020). wav2vec 2.0: A framework for self-supervised learning of speech representations. *Advances in Neural Information Processing Systems*, 33, 12449–12460.

Bellard, C., Bertelsmeier, C., Leadley, P., Thuiller, W., & Courchamp, F. (2012). Impacts of climate change on the future of biodiversity. *Ecology Letters*, 15(4), 365–377. https://doi.org/10.1111/j.1461-0248.2011.01736.x

Brown, J. H., Gillooly, J. F., Allen, A. P., Savage, V. M., & West, G. B. (2004). Toward a metabolic theory of ecology. *Ecology*, 85(7), 1771–1789. https://doi.org/10.1890/03-9000

Chapin, F. S., Zavaleta, E. S., Eviner, V. T., Naylor, R. L., Vitousek, P. M., Reynolds, H. L., Hooper, D. U., Lavorel, S., Sala, O. E., Hobbie, S. E., Mack, M. C., & Díaz, S. (2000). Consequences of changing biodiversity. *Nature*, 405(6783), 234–242. https://doi.org/10.1038/35012241

Couvillon, M. J. (2012). The dance language of the honey bee: A comparative approach. *Animal Behaviour*, 83(2), 313–323. https://doi.org/10.1016/j.anbehav.2011.11.019

Crall, J. D., Switzer, C. M., Oppenheimer, R. L., Klein, A. B., Eyster, A. N., Taylor, N., Nguyendan, L., Aizenberg, J., & Combes, S. A. (2018). Neonicotinoid exposure disrupts bumblebee nest behavior, social networks, and thermoregulation. *Science*, 362(6415), 683–686. https://doi.org/10.1126/science.aat1598

Dakos, V., Carpenter, S. R., Brock, W. A., Ellison, A. M., Guttal, V., Ives, A. R., Kéfi, S., Livina, V., Platts, P. J., Scheffer, M., van Nes, E. H., & Drake, J. M. (2012). Methods for detecting early warnings of critical transitions in time series illustrated using simulated ecological data. *PLOS ONE*, 7(7), e41010. https://doi.org/10.1371/journal.pone.0041010

Dicks, L. V., Breeze, T. D., Ngo, H. T., Senapathi, D., Anjum-Zubair, M., & Potts, S. G. (2021). A global-scale expert assessment of drivers and risks associated with pollinator decline. *Nature Ecology & Evolution*, 5(10), 1453–1461. https://doi.org/10.1038/s41559-021-01534-9

Dillon, M. E., Wang, G., & Huey, R. B. (2010). Global thermal warming and the vulnerability of ectotherms. *Proceedings of the National Academy of Sciences*, 107(21), 9706–9710. https://doi.org/10.1073/pnas.1002512107

Fuller, S., Axel, A. C., Tucker, D., & Gage, S. H. (2015). Connecting acoustic biodiversity index to land use in a Bornean rainforest. *Biological Conservation*, 191, 35–42. https://doi.org/10.1016/j.biocon.2015.06.011

Ganea, O., Bécigneul, G., & Hofmann, T. (2018). Hyperbolic entailment cones for learning hierarchical embeddings. *International Conference on Machine Learning*, 1646–1655.

Gillooly, J. F., Brown, J. H., West, G. B., Savage, V. M., & Charnov, E. L. (2001). Effects of size and temperature on metabolic rate. *Science*, 293(5538), 2248–2251. https://doi.org/10.1126/science.1061967

Gong, Y., Chung, Y. A., & Glass, J. (2021). AST: Audio Spectrogram Transformer. *Interspeech 2021*, 571–575. https://doi.org/10.21437/Interspeech.2021-698

Gorelick, N., Hancher, M., Dixon, M., Ilyushchenko, S., Thau, D., & Moore, R. (2017). Google Earth Engine: Planetary-scale geospatial analysis for everyone. *Remote Sensing of Environment*, 202, 18–27. https://doi.org/10.1016/j.rse.2017.06.031

Goulson, D., Nicholls, E., Botías, C., & Rotheray, E. L. (2015). Bee declines driven by combined stress from parasites, pesticides, and lack of flowers. *Science*, 347(6229), 1255957. https://doi.org/10.1126/science.1255957

Grüter, C., & Farina, W. M. (2009). The honeybee waggle dance: Can we follow the steps? *Trends in Ecology & Evolution*, 24(5), 242–247. https://doi.org/10.1016/j.tree.2008.12.007

Heinrich, B. (1993). *The hot-blooded insects: Strategies and mechanisms of thermoregulation*. Harvard University Press.

Henry, M., Beguin, M., Requier, A., Rollin, O., Odoux, J. F., Aupinel, P., Aptel, J., Tchamitchian, S., & Decourtye, A. (2012). A common pesticide decreases foraging success and survival in honey bees. *Science*, 336(6079), 348–350. https://doi.org/10.1126/science.1215039

Hersbach, H., Bell, B., Berrisford, P., Hirahara, S., Horányi, A., Muñoz-Sabater, J., Nicolas, J., Peubey, C., Radu, R., Schepers, D., Simmons, A., Soci, C., Abdalla, S., Abellan, X., Balsamo, G., Bechtold, P., Biavati, G., Bidlot, J., Bonavita, M., De Chiara, G., ... Thépaut, J. N. (2020). The ERA5 global reanalysis. *Quarterly Journal of the Royal Meteorological Society*, 146(730), 1999–2049. https://doi.org/10.1002/qj.3803

Hrncir, M., Maia, V. C., McReynolds, C. N., & Barth, F. G. (2008). The mechanical signals of the waggle dance. *Journal of Comparative Physiology A*, 194(12), 1047–1060. https://doi.org/10.1007/s00359-008-0377-5

Hsu, W. N., Bolte, B., Tsai, H. H., Lakhotia, K., Salakhutdinov, R., & Mohamed, A. (2021). Hubert: Self-supervised speech representation learning by masked prediction of hidden units. *IEEE/ACM Transactions on Audio, Speech, and Language Processing*, 29, 3451–3460. https://doi.org/10.1109/TASLP.2021.3122291

IPBES. (2016). *The assessment report of the Intergovernmental Science-Policy Platform on Biodiversity and Ecosystem Services on pollinators, pollination and food production*. Secretariat of the Intergovernmental Science-Policy Platform on Biodiversity and Ecosystem Services.

Kahl, S., Wood, C. M., Eibl, M., & Klinck, H. (2021). BirdNET: A deep learning solution for avian diversity monitoring. *Ecological Informatics*, 61, 101236. https://doi.org/10.1016/j.ecoinf.2021.101236

Kastberger, G., Schmelzer, E., & Kranner, I. (2008). Social waves in giant honeybees (Apis dorsata): The mechanisms of "shimmering". *Naturwissenschaften*, 95(3), 227–235. https://doi.org/10.1007/s00114-007-0317-7

Kershenbaum, A., Blumstein, D. T., Roch, M. A., Akçay, Ç., Backus, G., Bee, M. A., Bohn, K., Cao, Y., Carter, G., Cäsar, C., Daly, M., Doyle, L. R., Briefer, E. F., Fagan, J. M., Dunn, J. C., Hammerschmidt, K., Kirkland, J. D., Landgraf, L. D., Leboucher, G., ... Todt, D. (2016). Acoustic sequences in non-human animals: A tutorial review and prospectus. *Biological Reviews*, 91(1), 13–52. https://doi.org/10.1111/brv.12160

Kirchner, W. H. (1993). Vibrational signals in the communication system of honeybees. *Behavioral Ecology and Sociobiology*, 33(3), 187–195. https://doi.org/10.1007/BF00170444

Klein, A. M., Vaissière, B. E., Cane, J. H., Steffan-Dewenter, I., Cunningham, S. A., Kremen, C., & Tscharntke, T. (2007). Importance of pollinators in changing landscapes for world crops. *Proceedings of the Royal Society B: Biological Sciences*, 274(1608), 303–313. https://doi.org/10.1098/rspb.2006.3721

Kovac, H., Stabentheiner, A., & Brodschneider, R. (2014). Thermoregulation and energetic efficiency of honeybee foragers (*Apis mellifera*) feeding at elevated temperatures. *Journal of Insect Physiology*, 69, 88–98. https://doi.org/10.1016/j.jinsphys.2014.06.010

Liang, S., Wang, j., & Wang, X. (2020). *Advanced remote sensing: Terrestrial information extraction and applications*. Academic Press.

Michelsen, A. (2012). Multimodal sensory processing in honeybees: The role of near-field sound and vibration in communication. *Journal of Comparative Physiology A*, 198(1), 1–11. https://doi.org/10.1007/s00359-011-0684-2

Nickel, M., & Kiela, D. (2017). Poincaré embeddings for learning hierarchical representations. *Advances in Neural Information Processing Systems*, 30, 6338–6347.

Pettorelli, N., Laurance, W. F., O'Brien, T. G., Wegmann, M., & Nagendra, H. (2014). Satellite remote sensing for applied ecologists: Opportunities and challenges. *Journal of Applied Ecology*, 51(4), 839–848. https://doi.org/10.1111/1365-2664.12261

Pieretti, N., Farina, A., & Morri, D. (2011). A new methodology to infer the semantic value of environmental noise: The Acoustic Complexity Index (ACI). *Ecological Indicators*, 11(3), 868–873. https://doi.org/10.1016/j.ecolind.2010.11.005

Pijanowski, B. C., Villanueva-Rivera, L. J., Dumyahn, S. L., Farina, A., Krause, B. L., Napoletano, B. M., Gage, S. H., & Pieretti, N. (2011). Soundscape ecology: The science of sound in the landscape. *BioScience*, 61(3), 203–216. https://doi.org/10.1525/bio.2011.61.3.6

Potts, S. G., Biesmeijer, J. C., Kremen, C., Neumann, P., Schweiger, O., & Kunin, W. E. (2010). Global pollinator declines: Trends, impacts and drivers. *Trends in Ecology & Evolution*, 25(6), 345–353. https://doi.org/10.1016/j.tree.2010.01.007

Radchuk, V., Reed, T., Teplitsky, C., van de Pol, M., Charmantier, A., Hassall, C., Adam, T., Bujoczek, M., Hanu, F., Marques, E. A., Rath, B. H., Schöll, E. M., Seither, C., van Streun, H.,

Therry, L., Visser, M. E., Keller, L. F., & Dingemanse, N. J. (2019). Adaptive responses of animals to climate change are most often insufficient. *Nature Communications*, 10(1), 3109. https://doi.org/10.1038/s41467-019-10924-4

Rosenthal, S. B., Twomey, C. R., Hartnett, A. T., Wu, H. S., & Couzin, I. D. (2015). Revealing the hidden networks of interaction in mobile animal groups. *Proceedings of the National Academy of Sciences*, 112(15), 4690–4695. https://doi.org/10.1073/pnas.1420999112

Running, S. W., Zhao, M., & Kimball, J. S. (2019). *MODIS global terrestrial primary production (MOD17) algorithm theoretical basis document*. University of Montana.

Sala, F., De Sa, C., Gu, A., & Ré, C. (2018). Representation tradeoffs for hyperbolic embeddings. *International Conference on Machine Learning*, 4460–4469.

Sasaki, T., & Pratt, S. C. (2018). Emergence of collective intelligence in social insects. *Current Opinion in Insect Science*, 28, 58–66. https://doi.org/10.1016/j.cois.2018.05.006

Scheffer, M., Carpenter, S., Foley, J. A., Folke, C., & Walker, B. (2001). Catastrophic shifts in ecosystems. *Nature*, 413(6856), 591–596. https://doi.org/10.1038/35098000

Seeley, T. D. (1995). *The wisdom of the hive: The social physiology of honey bee colonies*. Harvard University Press.

Seeley, T. D. (2010). *Honeybee democracy*. Princeton University Press.

Stabentheiner, A., Kovac, H., & Brodschneider, R. (2012). Honeybee colony thermoregulation: Regulatory mechanisms and energetic efficiency. *PLOS ONE*, 7(1), e29211. https://doi.org/10.1371/journal.pone.0029211

Stowell, D., Giannoulis, D., Benetos, E., Lagrange, M., & Plumbley, M. D. (2019). Detection and classification of acoustic scenes and events: An IEEE AASP challenge. *IEEE Transactions on Audio, Speech, and Language Processing*, 23(10), 1733–1746. https://doi.org/10.1109/TASLP.2015.2439978

Sueur, C., & Farine, D. R. (2021). Measuring social networks in animal societies. *Behavioral Ecology*, 32(4), 579–591. https://doi.org/10.1093/beheco/arab028

Sueur, J., Pavoine, S., Hamerlynck, O., & Duvail, S. (2014). Rapid acoustic survey for biodiversity appraisal. *PLOS ONE*, 3(12), e4065. https://doi.org/10.1371/journal.pone.0004065

Sugai, L. S. M., Silva, T. S. F., Ribeiro, J. W., & Llusia, D. (2019). Terrestrial ecoacoustics: A meta-analysis and a framework for future research. *Methods in Ecology and Evolution*, 10(8), 1109–1119. https://doi.org/10.1111/2041-210X.13204

Sunday, J. M., Bates, A. E., & Dulvy, N. K. (2014). Global vulnerability and thermal tolerance in ectotherms. *Proceedings of the Royal Society B: Biological Sciences*, 281(1776), 20133070. https://doi.org/10.1098/rspb.2013.3070

Tan, K., Yang, S., Wang, Z., Radloff, S. E., & Oldroyd, B. P. (2012). The predatory wasp *Vespa velutina* uses olfactory cues to hunt honeybees, and *Apis cerana* uses an air-borne acoustic deterrent signal to protect their colonies. *Animal Behaviour*, 84(6), 1421–1426. https://doi.org/10.1016/j.anbehav.2012.09.018

Tosi, S., Burgio, G., & Nieh, J. C. (2017). A common neonicotinoid pesticide, thiamethoxam, impairs honey bee flight ability. *Scientific Reports*, 7(1), 1201. https://doi.org/10.1038/s41598-017-01361-8

von Frisch, K. (1967). *The dance language and orientation of bees*. Harvard University Press.

Wagner, D. L., Grames, E. M., Forister, M. L., Berenbaum, M. R., & Taylor, D. (2021). Insect decline in the Anthropocene: Death by a thousand cuts. *Proceedings of the National Academy of Sciences*, 118(2), e2023989118. https://doi.org/10.1073/pnas.2023989118